NACA RM L9H08

NACA

RESEARCH MEMORANDUM

AN EMPIRICAL METHOD FOR ESTIMATING TRAILING-EDGE LOADS AT TRANSONIC SPEEDS

By T. H. Skopinski

Langley Aeronautical Laboratory
Langley Air Force Base, Va.

NATIONAL ADVISORY COMMITTEE
FOR AERONAUTICS

WASHINGTON

October 6, 1949

NACA RM L9H08

NATIONAL ADVISORY COMMITTEE FOR AERONAUTICS

RESEARCH MEMORANDUM

AN EMPIRICAL METHOD FOR ESTIMATING TRAILING-EDGE LOADS AT TRANSONIC SPEEDS

By T. H. Skopinski

SUMMARY

An analysis of selected experimental pressure-distribution data at transonic speeds has been made for the purpose of deriving an empirical method which may be used for estimating the trailing-edge loads and bending moments at the design stage.

The results presented indicate that the trailing-edge normal-force and bending-moment coefficients calculated by the derived method follow the general trend of the experimental data and appear to be a guide where specifically applicable chordwise pressure-distribution data at transonic speeds are not available. The experimental data indicate that two suggested methods now being used to establish the intensity and air-load distribution over the trailing edge are not valid in the entire transonic range for a wide lift-coefficient range and variation of airfoil types. Symmetrical airfoils with maximum thickness at or near midchord appear to reduce the trailing-edge loads and bending moments associated with transonic speeds.

INTRODUCTION

The tendency toward thinner wings and the rearward movement of the loads center with increasing speeds makes the design of the overhanging or trailing-edge portion of the airfoil more important than heretofore. At present, the most satisfactory method for designing the trailing-edge portion is by recourse to measured pressure distributions covering the desired range of Mach number and lift coefficients for the particular airfoil section. An alternative and acceptable method when speeds are below the critical is to use computed pressure distributions.

The usual case, however, is generally an exception to the preceding case so that these obvious methods cannot be employed, and it then becomes necessary to use either empirical rules or be guided by results

from nearly comparable data. Since the problem of determining the trailing-edge load is related to a number of variables such as Reynolds number, Mach number, angle of attack, airfoil section, roughness, trailing-edge angle, and so forth, it is immediately apparent that existing data are not sufficient to establish fine guides which will allow all of these effects to be separated, any more than it is possible to do so for hinge-moment data.

At present there are available two suggestions for design requirements in the transonic range which may be used to establish the intensity of the loading over the trailing edge. Both of these are based on experimental results obtained over a particular airfoil section and cover only limited range of Mach number and lift. The purpose of this paper is to analyze existing data regardless of range of Mach number or section in order to establish a more general empirical guide which may be used where either experimental data or available methods for computing the pressure distributions are inadequate.

The method derived is based primarily on the analysis of the pressure distributions obtained from 15 different NACA airfoils, covering all general types and, insofar as possible, other geometric variables. This paper presents a comparison of the experimental trailing-edge loads with those obtained by use of the derived method. Also presented for comparison are results obtained from requirements now being used.

SYMBOLS

M	Mach number
R	Reynolds number
α	angle of attack, degrees
c	section chord, feet
c_f	chord of trailing edge considered, fraction of section chord
x	distance along chord from leading edge of airfoil section, fraction of chord
p_o	static pressure in undisturbed stream, pounds per square foot
p	local static pressure at point on airfoil section, pounds per square foot

[redacted]

q	dynamic pressure, pounds per square foot
P	pressure coefficient $\left(\frac{p - p_o}{q}\right)$
t	maximum thickness of section, feet
t/c	thickness ratio
c_n	section normal-force coefficient
c_{n_f}	trailing-edge normal-force coefficient based on c_f
c_{M_f}	trailing-edge bending-moment coefficient of trailing-edge normal force taken about (1.0 - c_f) point
K	empirical constant to include effect of camber on trailing-edge load
X	empirical constant to include effect of camber on trailing-edge load distribution

Subscripts:

o	free stream
L	lower surface
U	upper surface
cr	critical

AIRFOILS SELECTED

The airfoils selected for analysis are listed in table I. The selections made cover the various types such as the NACA 4- and 5-digit series, the laminar-flow, and the supersonic airfoils. Within each type, an attempt has been made to make the selection so that a range of thickness ratio and camber would be represented and at the same time an adequate range of Mach number and angle of attack could be covered. Although this latter stipulation was made, experimental pressure distributions for Mach numbers above 0.85 covering a wide lift-coefficient range are very meager due to either limitations resulting from model strength requirements or to the validity of wind-tunnel data near choking speeds. Airfoils in group 1 represent supersonic airfoils;

whereas airfoils in group 2 represent laminar-flow airfoils where thickness and camber are varied. Airfoils of group 3 include variations both in type and series.

EVALUATION OF DATA AND SUGGESTED METHODS

The evaluation of the data consisted of integrating pressure distributions such as are given in figures 1 and 2 over the rear 20, 25, and 30 percent of the chord at various Mach numbers and airfoil normal-force coefficients. The results of these integrations are given in figures 3(a) to 3(o) where the normal-force coefficient of the rear portion based on the equation

$$c_{n_f} = \frac{1}{c_f} \int_{1.0-c_f}^{1.0} (P_L - P_U) dx$$

is plotted against Mach number with chord ratio and normal-force coefficient as parameters.

Similarly, the moment coefficient of the trailing-edge load about the selected positions was also determined by graphical integration. These results are given in figures 4(a) to 4(o) where the bending-moment coefficient, defined by the equation

$$c_{M_f} = -\frac{1}{c_f^2} \int_{1.0-c_f}^{1.0} (P_L - P_U) \left[x - (1 - c_f)\right] dx$$

is plotted against Mach number with section normal-force coefficient and chord ratio as parameters.

Using the experimental results in figures 3 and 4, an empirical method has been derived to predict the general behavior and magnitude of the trailing-edge normal-force and bending-moment coefficients over at least the aft 30 percent of the airfoil sections in the entire transonic region. The variables used would be available at the design stage and include thickness ratio, section normal-force coefficient, camber, Mach number, and the magnitude at subcritical speeds of the trailing-edge normal-force and bending-moment coefficients for a

specific type of airfoil section. The derived equations and constants are as follows:

For $\frac{t}{c} \geqq 0.13$ and $M = 0.70$ to $M = 1.0$

$$c_{n_f} = \left(\frac{M - 0.70}{0.30}\right)\left[(c_n + K) - (c_{n_f})_{M=0.60}\right] + (c_{n_f})_{M=0.60} \tag{1a}$$

For $\frac{t}{c} \geqq 0.10 < 0.13$ and $M = 0.75$ to $M = 1.0$

$$c_{n_f} = \left(\frac{M - 0.75}{0.25}\right)\left[(c_n + K) - (c_{n_f})_{M=0.60}\right] + (c_{n_f})_{M=0.60} \tag{1b}$$

For $\frac{t}{c} < 0.10$ and $M = 0.80$ to $M = 1.0$

$$c_{n_f} = \left(\frac{M - 0.80}{0.20}\right)\left[(c_n + K) - (c_{n_f})_{M=0.60}\right] + (c_{n_f})_{M=0.60} \tag{1c}$$

For $M = 1.0$ to $M = 1.5$

$$c_{n_f} = (c_n + K)\left(1 - \frac{M - 1.0}{4}\right) \tag{1d}$$

For $\frac{t}{c} \geqq 0.13$ and $M = 0.70$ to $M = 1.0$

$$c_{M_f} = -\left(\frac{M - 0.70}{0.30}\right)\left[(c_n + K)X + (c_{M_f})_{M=0.60}\right] + (c_{M_f})_{M=0.60} \tag{2a}$$

For $\frac{t}{c} \geqq 0.10 < 0.13$ and $M = 0.75$ to $M = 1.0$

$$c_{M_f} = -\left(\frac{M - 0.75}{0.25}\right)\left[(c_n + K)X + (c_{M_f})_{M=0.60}\right] + (c_{M_f})_{M=0.60} \tag{2b}$$

For $\frac{t}{c} < 0.10$ and $M = 0.80$ to $M = 1.0$

$$c_{M_f} = -\left(\frac{M - 0.80}{0.20}\right)\left[(c_n + K)X + (c_{M_f})_{M=0.60}\right] + (c_{M_f})_{M=0.60} \tag{2c}$$

[redacted]

For $M = 1.0$ to $M = 1.5$

$$c_{M_f} = -Xc_{n_f} \tag{2d}$$

where

$K = 0$ for symmetrical airfoils

$K = 0.10$ for up to 2-percent cambered airfoils

$K = 0.20$ for greater than 2-percent cambered airfoils

$X = 0.50$ for symmetrical airfoils

$X = 0.55$ for cambered airfoils

The empirical constants K and X were determined to account for the effects of camber on the trailing-edge load and load distribution at zero lift. The values for c_{n_f} and c_{M_f} for $M = 0.60$ are obtained for each specific type of airfoil section at various section normal-force coefficients either from experimental results or from acceptable analytical methods. Since the magnitude of c_{n_f} and c_{M_f} for a given section normal-force coefficient will not vary appreciably below the critical Mach number, the subcritical values of c_{n_f} and c_{M_f} may be used when experimental data at $M = 0.60$ are not available for a specific type of airfoil section or when M_{cr} is below 0.60. For Mach numbers greater than unity, the trailing-edge normal-force- and bending-moment-coefficient trends obtained on several circular-arc profiles by the semiempirical method of reference 7 were used as a basis of determining equations 1(d) and 2(d).

Using equations (1) and (2), the trailing-edge normal-force and bending-moment coefficients are plotted as lines A in figures 3 and 4, respectively, as a function of Mach number with section normal-force coefficient as the parameter.

For purposes of comparison, results calculated by two previously suggested methods are also included in figures 3 and 4 as curves B and lines C. The results shown by curve B were obtained from an empirical method suggested by the Bureau of Aeronautics, Department of the Navy, which was based largely on the experimental results of reference 8. The method is intended to predict the loads for at least the aft 30 percent of the airfoil section. For the trailing-edge normal-force coefficient, a compressibility increment Δc_{n_f} defined by the empirical formula

$$\Delta c_{n_f} = 0.35\left(\frac{M}{M_{cr}} - 1\right)^{1/2}$$

is added to the value of the normal-force coefficient of the trailing-edge portion considered at M_{cr} or $M = 0.60$, whichever is the greater. For values of M/M_{cr} greater than 2.0 the value of this trailing-edge compressibility increment need not exceed 0.35.

Similarly, a compressibility bending-moment-coefficient increment Δc_{M_f} defined by the formula

$$\Delta c_{M_f} = -0.50 \Delta c_{n_f}$$

is added to the bending-moment-coefficient value at M_{cr} or $M = 0.60$ when M_{cr} is below 0.60.

The results shown by line C in figures 3 and 4 are based on the recommendation in reference 4 that the aft 30 percent of the wing chord be designed for a uniform chordwise loading of $0.40q$ at supercritical Mach numbers. In the present case, then, line C in figure 3 has a constant value of 0.40 for c_{n_f} and in figure 4, a constant value of -0.20 for c_{M_f}.

DISCUSSION

From examination of figures 3 and 4 it can be seen that the trailing-edge normal-force- and bending-moment-coefficient results calculated by the method presented in this paper (lines A) follow the general trend of the experimental data. The experimental data are characterized by a flat portion at the lower Mach numbers followed by a rapid increase, which in most cases continued to the highest test Mach number. In the cases where the experimental data do not follow this trend, it was concluded that the deviations were caused by a large number of variables which could not be conveniently accounted for in a general empirical method. In view of the fact that the proposed empirical method, in general, showed a slight degree of conservatism even in these cases, it may be used as a guide when experimental data are not available.

The validity of the proposed empirical method for Mach numbers near and greater than unity might well be questioned since no experimental data in this range are presented for comparison. Indications from data not available for publication, however, show that the empirical method is as good a guide in this region as it is in the lower transonic Mach number range.

The two methods (curves B and lines C) suggested previously were not adequate for predicting the trailing-edge loads for the large variation of airfoil types, section normal-force coefficients, and Mach numbers shown. Since these two methods were based on limited experimental data, they could hardly be expected to predict the general trends which are observed only after a great deal of experimental transonic data are examined.

From the examination of the experimental trailing-edge normal-force- and bending-moment-coefficient data presented in figures 3 and 4 certain general trends can be observed. Below the critical Mach number the trailing-edge normal-force and bending-moment coefficients increase with chord ratio and section normal-force coefficient in accordance with theory. Above the critical Mach number this is not necessarily the case (see figs. 3(n) and 4(n)) as the normal force and bending moment on the trailing edge may actually decrease with these variables and the curves cross over. Apart from this difference in the relative position of the curves which occur above a given Mach number, there is the general tendency for the normal-force and bending-moment coefficients to increase rapidly to the highest Mach number reached in the tests. In some cases, however, (for example, figs. 3(g) and 4(g)) a peak is reached followed by a rapid drop and still a more rapid rise to the highest Mach number tested, but this effect seems to be minimized as the section normal force is increased. Although the effect of the numerous variables involved could not be isolated, it appears that symmetrical airfoils with maximum thickness at or near midchord reduce the trailing-edge loads and bending moments associated with transonic speeds.

Certain trends can also be observed within each group of airfoils considered. In group 1, the magnitude of the trailing-edge normal-force and bending-moment coefficients for the thin supersonic airfoils (figs. 3(a) to 3(c) and 4(a) to 4(c)) was small for Mach numbers below approximately 0.80. Moving the position of maximum thickness from the 30-percent-chord position to the 50-percent-chord position resulted in the change in sign of the loading and moment coefficient over various portions of the trailing edge. In group 2, the data for the laminar-flow airfoils (figs. 3(d) to 3(k) and 4(d) to 4(k)) indicate that the Mach number at which the initial rapid increase in the trailing-edge normal-force and bending-moment coefficient occurred was a function of the thickness ratio and, to a small extent, a function of the section normal-force coefficient. (For example, see figs. 3(f), 3(j), 4(f), and 4(j).) In group 3, the change in series data indicates that the highly cambered airfoils (figs. 3(l), 3(m), 4(l), and 4(m)) experience large trailing-edge loads and bending moments at the low-lift conditions as compared to the values obtained for the symmetrical and medium cambered conventional airfoils (figs. 3(n), 3(o), 4(n), and 4(o)).

CONCLUSIONS

The results of the analysis of the trailing-edge loads at transonic speeds indicated the following conclusions:

1. The trailing-edge normal-force and bending-moment coefficients calculated by the derived method follow the general trend of the experimental data and appear to be a guide where specifically applicable chordwise pressure-distribution data at transonic speeds are not available.

2. The two suggested methods now being used to establish the intensity and air-load distribution over the trailing edges of the airfoil sections are not adequate over the entire transonic range for a large variation of airfoil types and section normal-force coefficients.

3. Although the effects of the numerous variables involved could not be isolated, it appears that symmetrical airfoils with maximum thickness at or near the midchord reduce the trailing-edge loads and bending moments associated with transonic speeds.

Langley Aeronautical Laboratory
National Advisory Committee for Aeronautics
Langley Air Force Base, Va.

[redacted]

REFERENCES

1. Lindsey, W. F., Daley, Bernard N., and Humphreys, Milton D.: The Flow and Force Characteristics of Supersonic Airfoils at High Subsonic Speeds. NACA TN 1211, 1947.

2. Bielat, Ralph P.: Investigation at High Speeds of a Horizontal-Tail Model in the Langley 8-Foot High-Speed Tunnel. NACA RM L6L10b, 1947.

3. Whitcomb, Richard T.: Investigation of the Characteristics of a High-Aspect-Ratio Wing in the Langley 8-Foot High-Speed Tunnel. NACA RM L6H28a, 1946.

4. Brown, Harvey H., and Clousing, Lawrence A.: Wing Pressure-Distribution Measurements up to 0.866 Mach Number in Flight on a Jet-Propelled Airplane. NACA TN 1181, 1947.

5. Brown, Harvey H., Rolls, L. Steward, and Clousing, Lawrence A.: An Analysis of Longitudinal-Control Problems Encountered in Flight at Transonic Speeds with a Jet-Propelled Airplane. NACA RM A7G03, 1947.

6. Graham, Donald J., Nitzberg, Gerald E., and Olsen, Robert N.: A Systematic Investigation of Pressure Distributions at High Speeds over Five Representative NACA Low-Drag and Conventional Airfoil Sections. NACA RM A7B04, 1947.

7. Mayer, John P.: Estimation of Lift and Drag of Airfoils at Near Sonic Speeds and in the Presence of Detached Shock Waves. NACA RM L8L07, 1949.

8. Luoma, Arvo A.: An Investigation of a High-Aspect-Ratio Wing Having 0.20-Chord Plain Ailerons in the Langley 8-Foot High-Speed Tunnel. NACA RM L6H28d, 1946.

[redacted]

[redacted]

TABLE I

AIRFOILS SELECTED FOR ANALYSIS

Group	Airfoil section	M	$R \times 10^{-6}$	Reference
1	NACA 18(30)(03)-(30)(03)	0.30 to 0.90	0.70 to 1.5	1
	NACA 28(30)(03)-(30)(03)	0.30 to 0.90	0.70 to 1.5	1
	NACA 28(50)(03)-(50)(03)	0.30 to 0.90	0.70 to 1.5	1
2	NACA 66-006	0.30 to 0.90	0.70 to 1.5	1 and unpublished Langley rectangular high-speed-tunnel results
	NACA 65-108	0.40 to 0.925	1.25 to 1.9	2
	NACA 65-208	0.20 to 0.90	1.50 to 4.5	Unpublished data from Ames Aeronautical Laboratory
	NACA 65-210	0.40 to 0.925	0.90 to 1.4	3 and unpublished Langley 8-foot high-speed-tunnel results
	NACA 65-212	0.20 to 0.90	1.5 to 4.5	Unpublished data from Ames Aeronautical Laboratory
	NACA 65-213 (a=0.5)	0.70 to 0.86	20 to 36	4, 5, and unpublished data from Ames Aeronautical Laboratory
	NACA 65-215 (a=0.5)	0.30 to 0.85	1.0 to 2.0	6
	NACA 66,2-215 (a=0.6)	0.30 to 0.85	1.0 to 2.0	6
3	NACA 16-307	0.50 to 1.09	2.0 to 4.5	Unpublished Langley 16-foot high-speed-tunnel results
	NACA 4415	0.30 to 0.85	1.0 to 2.0	6
	NACA 0015	0.30 to 0.85	1.0 to 2.0	6
	NACA 23015	0.30 to 0.85	1.0 to 2.0	6

[redacted]

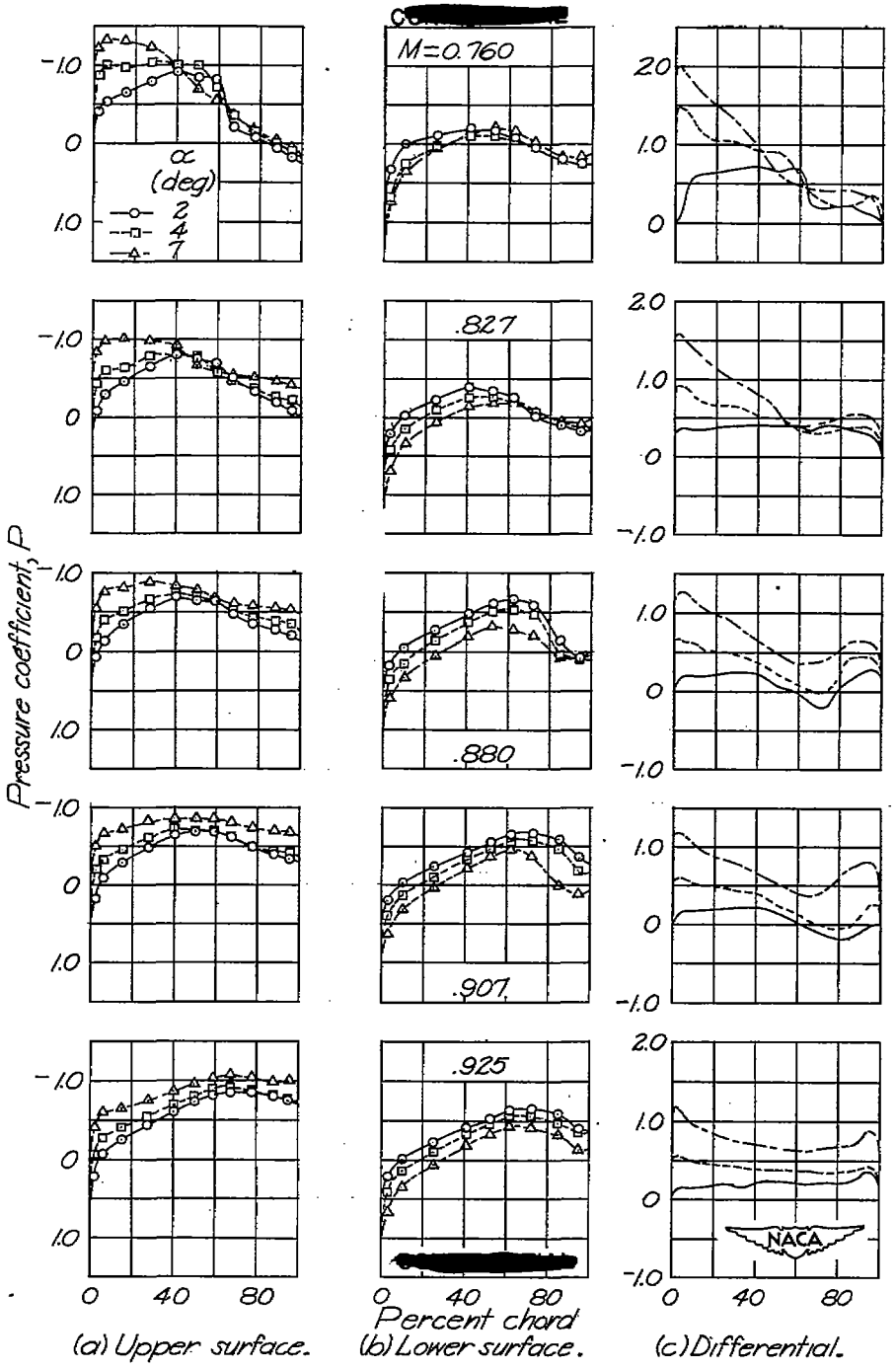

Figure 1.- Typical pressure distributions obtained for wing model having an NACA 65-210 airfoil section for various values of angle of attack and Mach number; 30-percent semispan station. (Reference 3 and unpublished Langley 8-foot high-speed-tunnel results.)

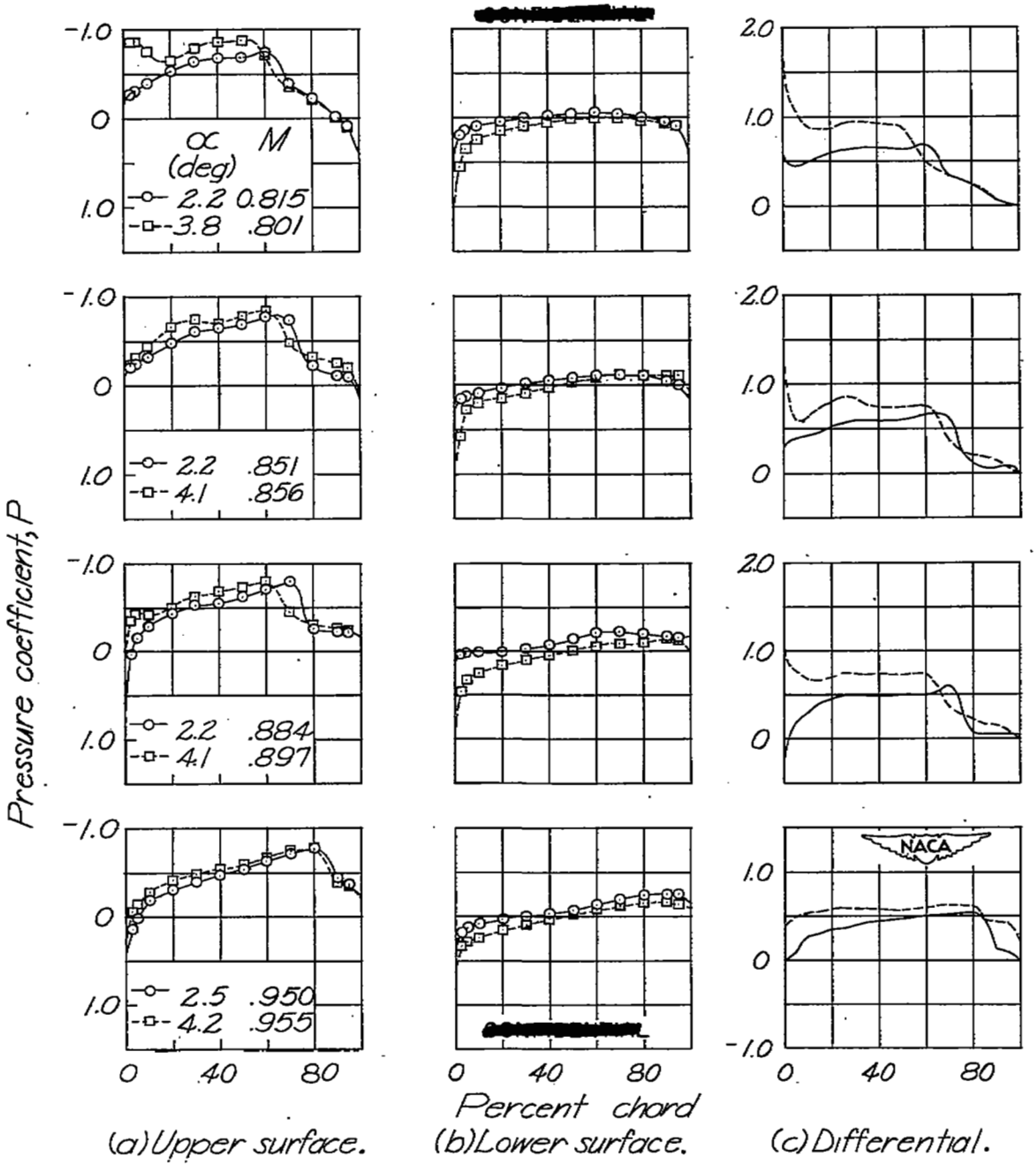

Figure 2.- Typical pressure distributions obtained for a propeller having an NACA 16-307 airfoil section at 80-percent radius station for various values of angle of attack and Mach number. (Unpublished Langley 16-foot high-speed-tunnel results.)

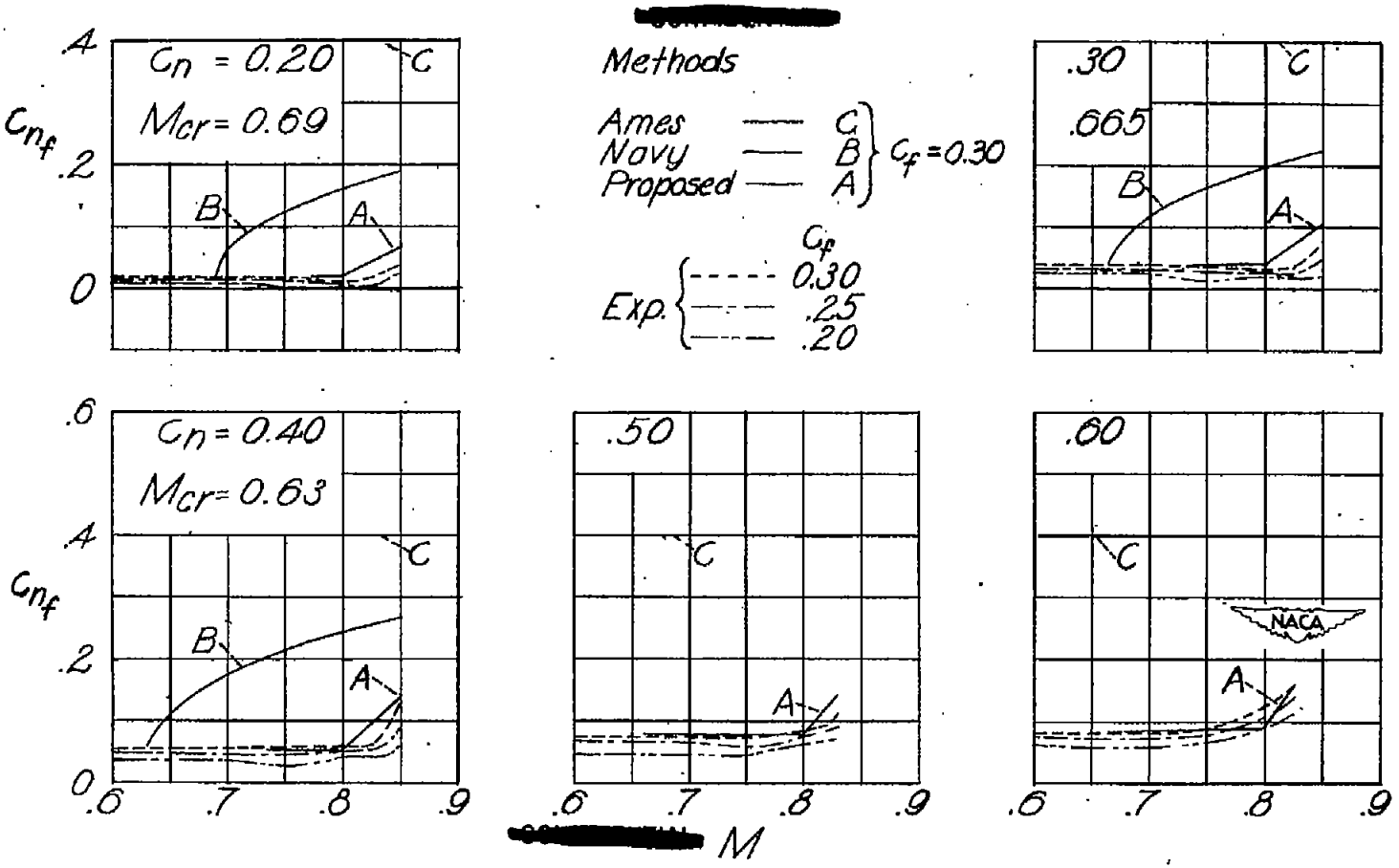

(a) NACA 1S(30)(03)-(30)(03) airfoil section. (Uncorrected results)

Figure 3.- Comparison of experimental and calculated trailing-edge normal-force coefficients.

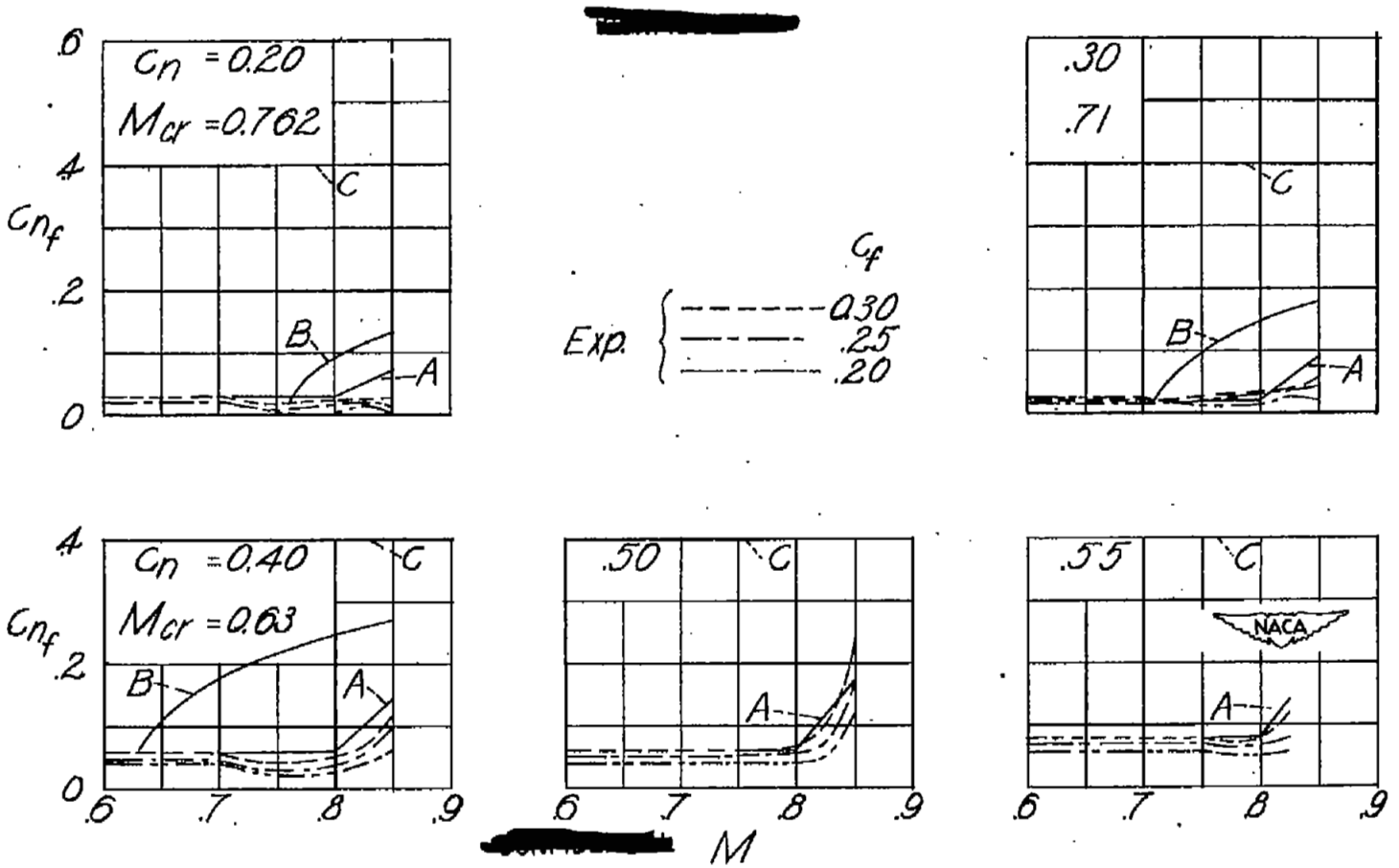

(b) NACA 2S(30)(03)-(30)(03) airfoil section. (Uncorrected results)

Figure 3.- Continued.

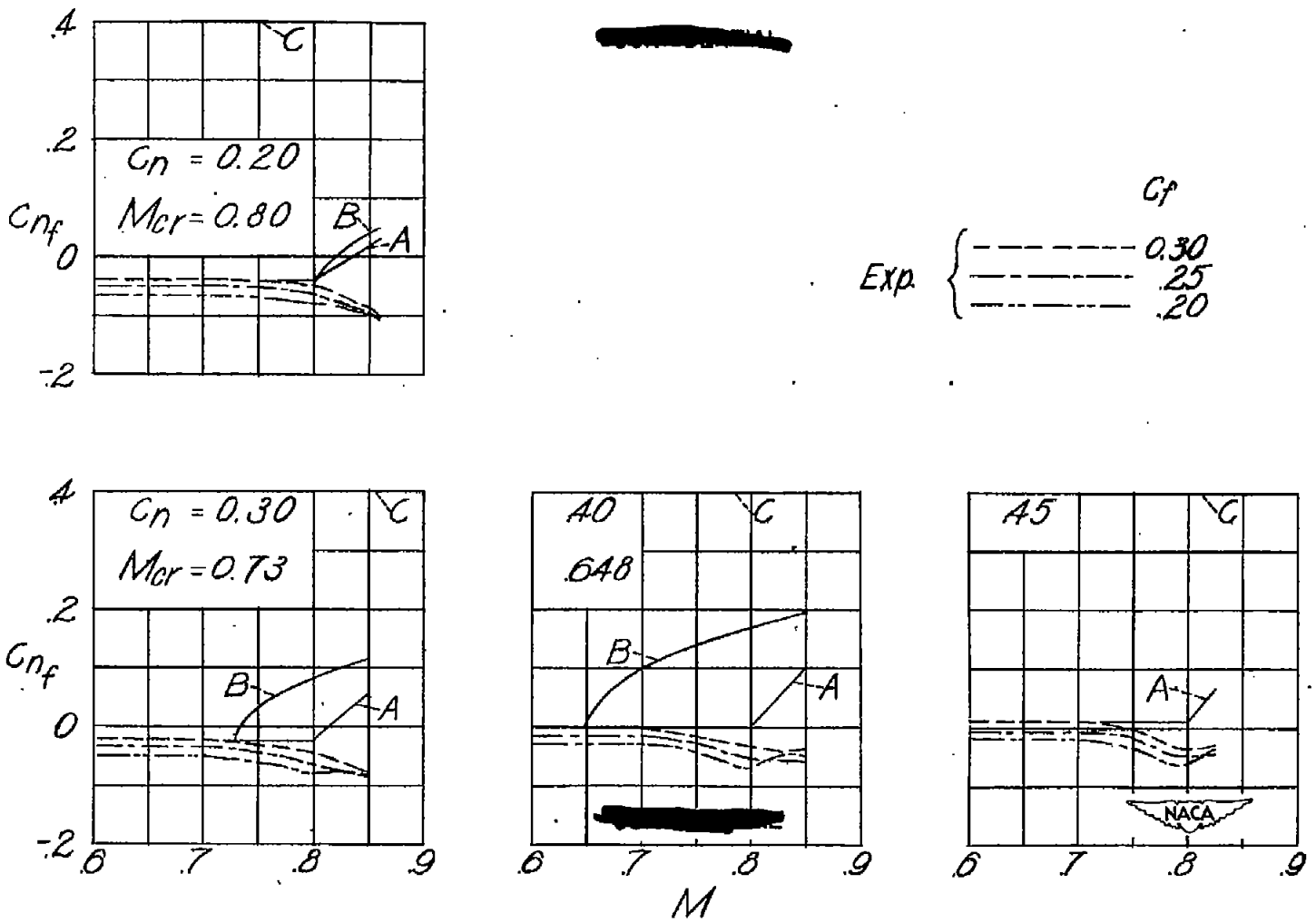

(c) NACA 2S(50)(03)-(50)(03) airfoil section. (Uncorrected results)

Figure 3.- Continued.

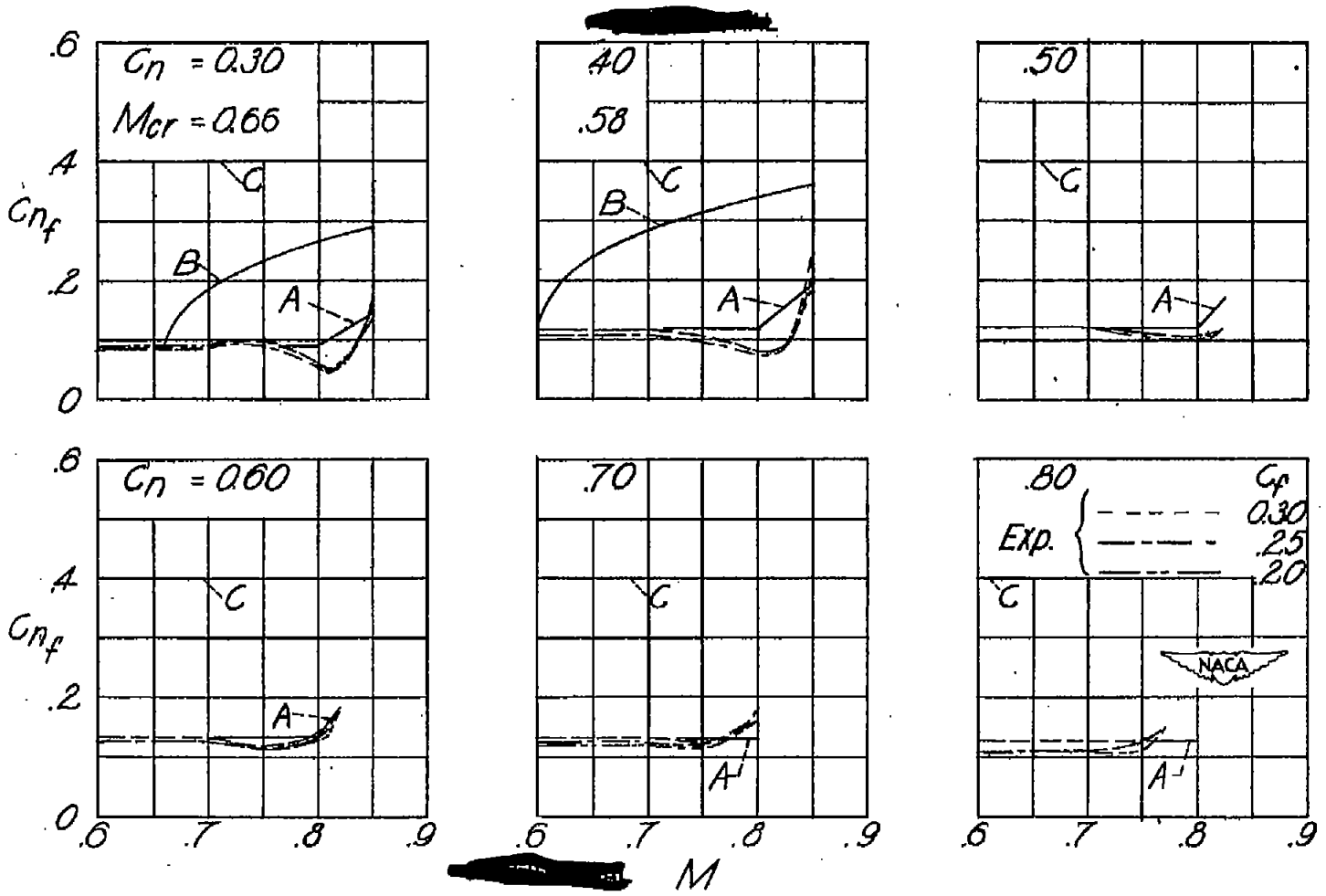

(d) NACA 66-006 airfoil section. (Uncorrected results)

Figure 3.- Continued.

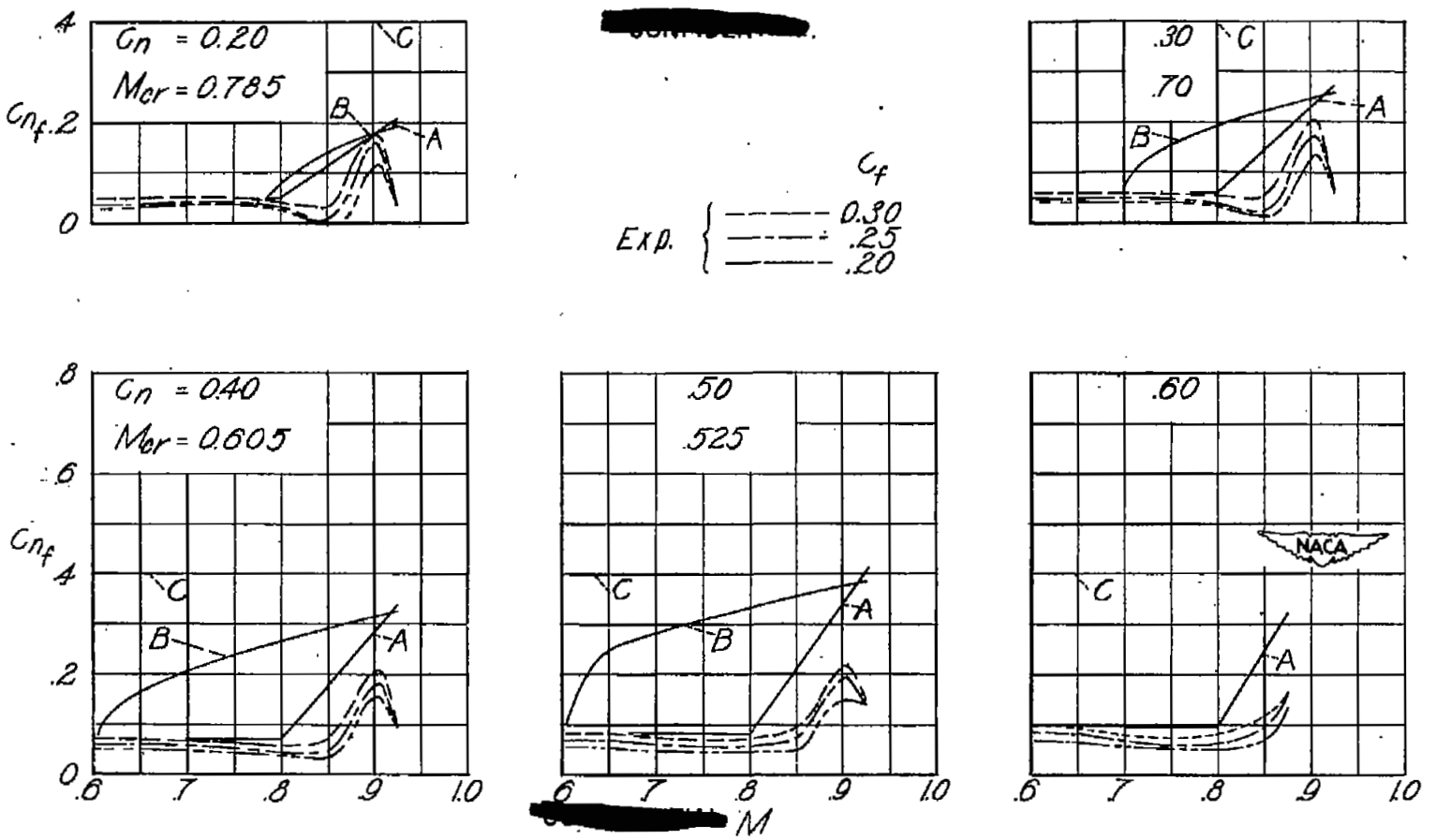

(e) Horizontal-tail model having an NACA 65-108 airfoil section equipped with a 0.30c plain elevator; 40-percent semispan station.

Figure 3.- Continued.

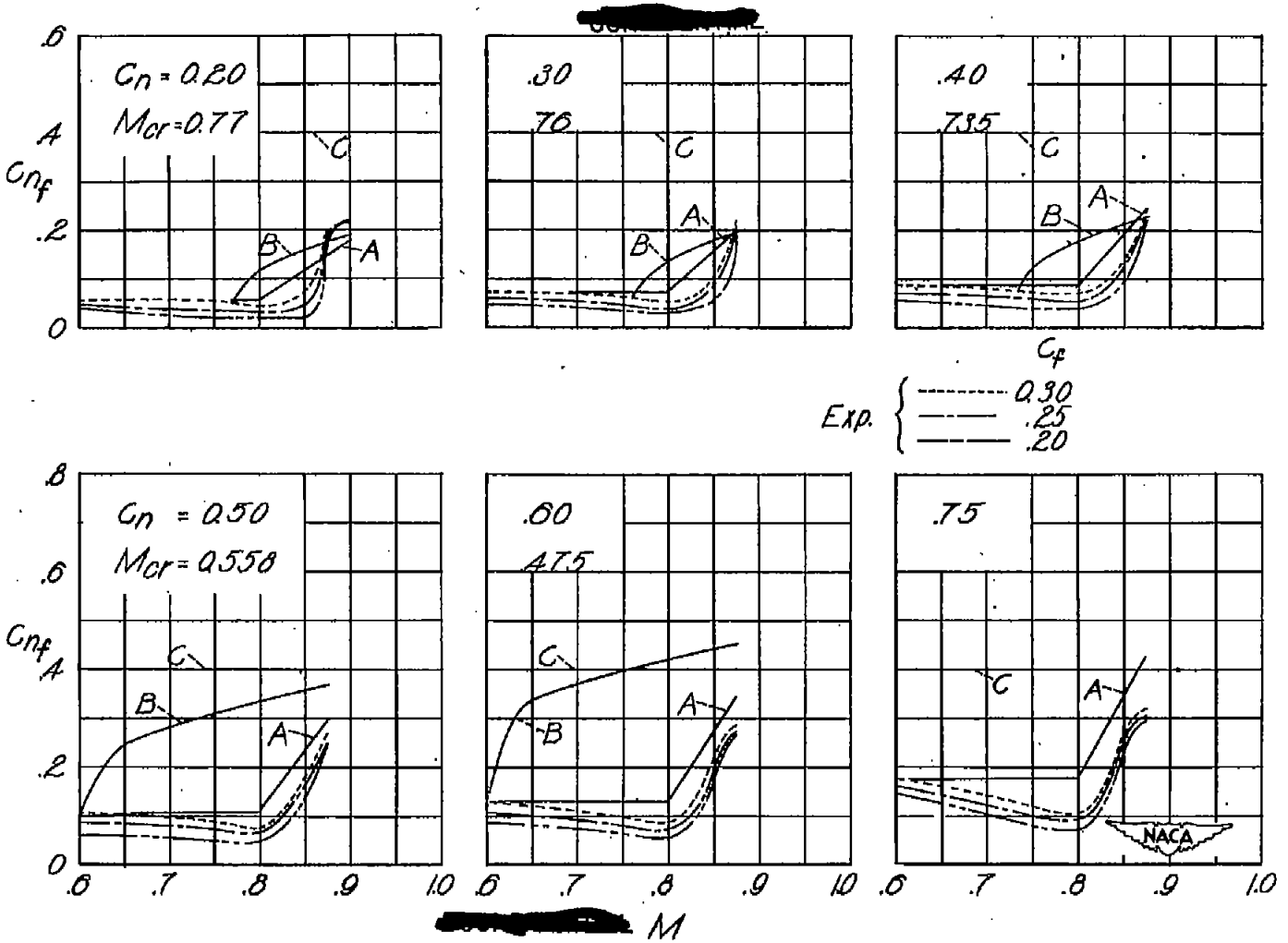

(f) Wing model having an NACA 65-208 airfoil section; 16-percent semispan station.

Figure 3.- Continued.

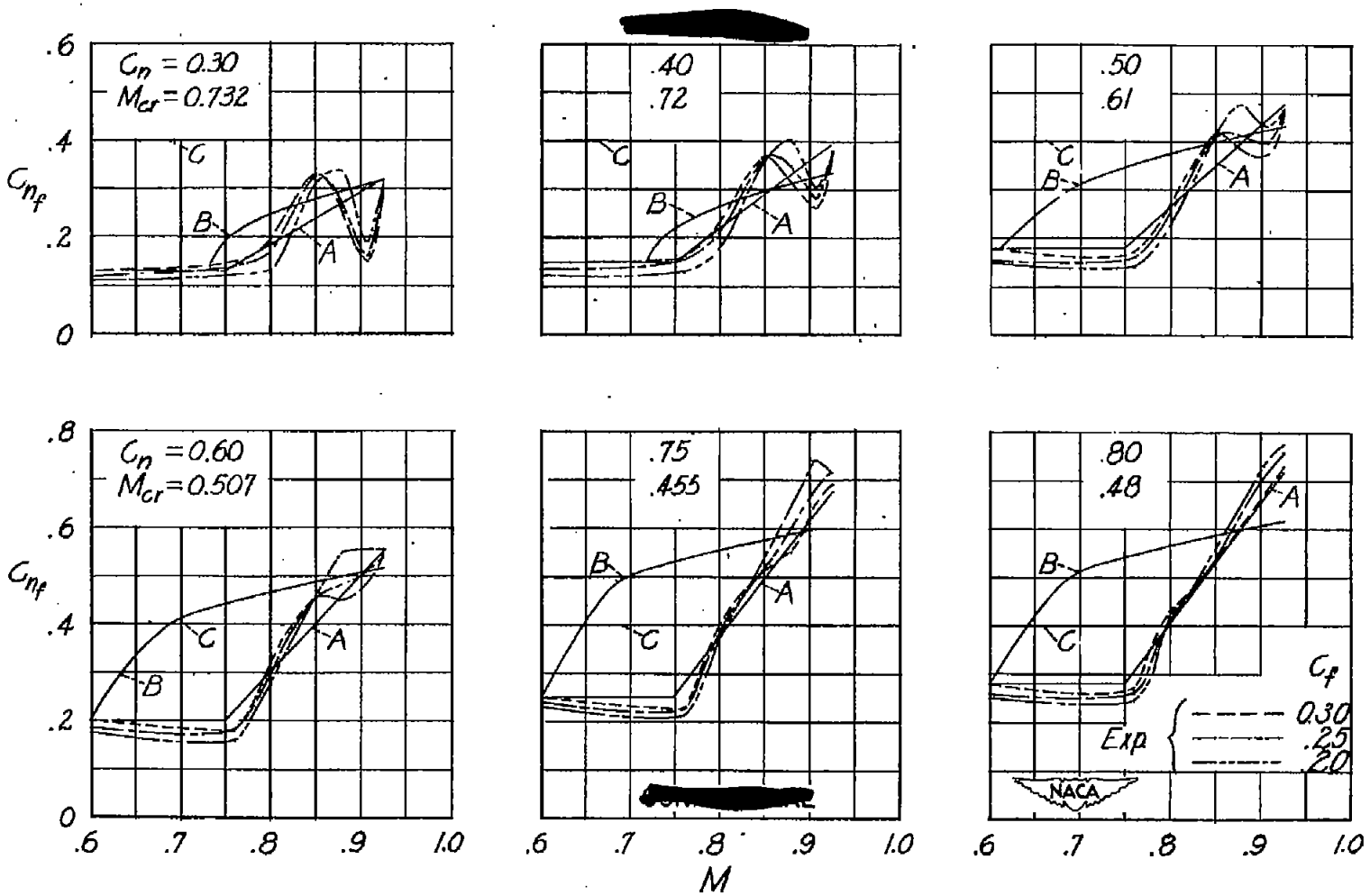

(g) Wing model having an NACA 65-210 airfoil; 30-percent semispan station.

Figure 3.- Continued.

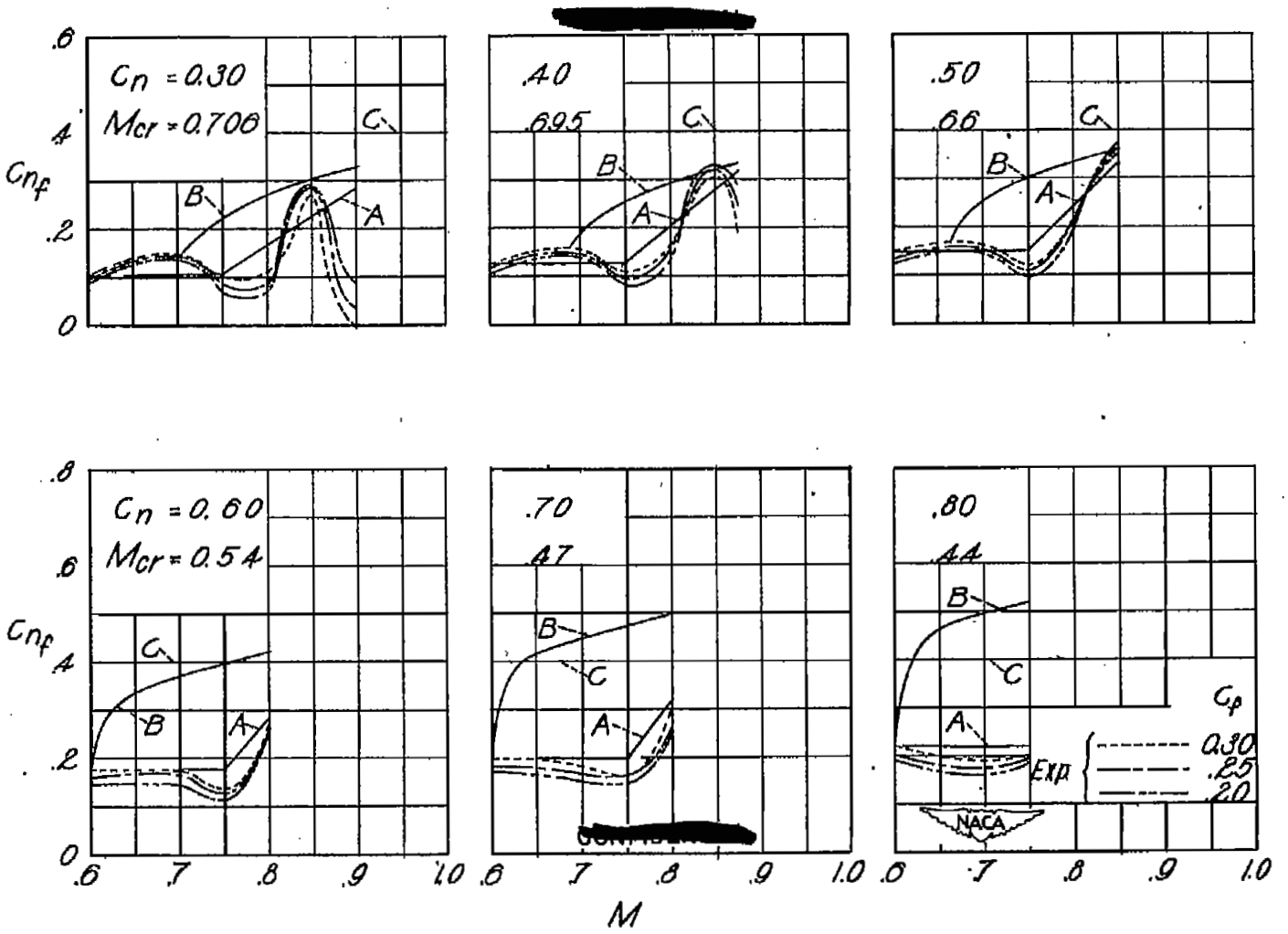

(h) Wing model having an NACA 65-212 airfoil section; 16-percent semispan station.

Figure 3.- Continued.

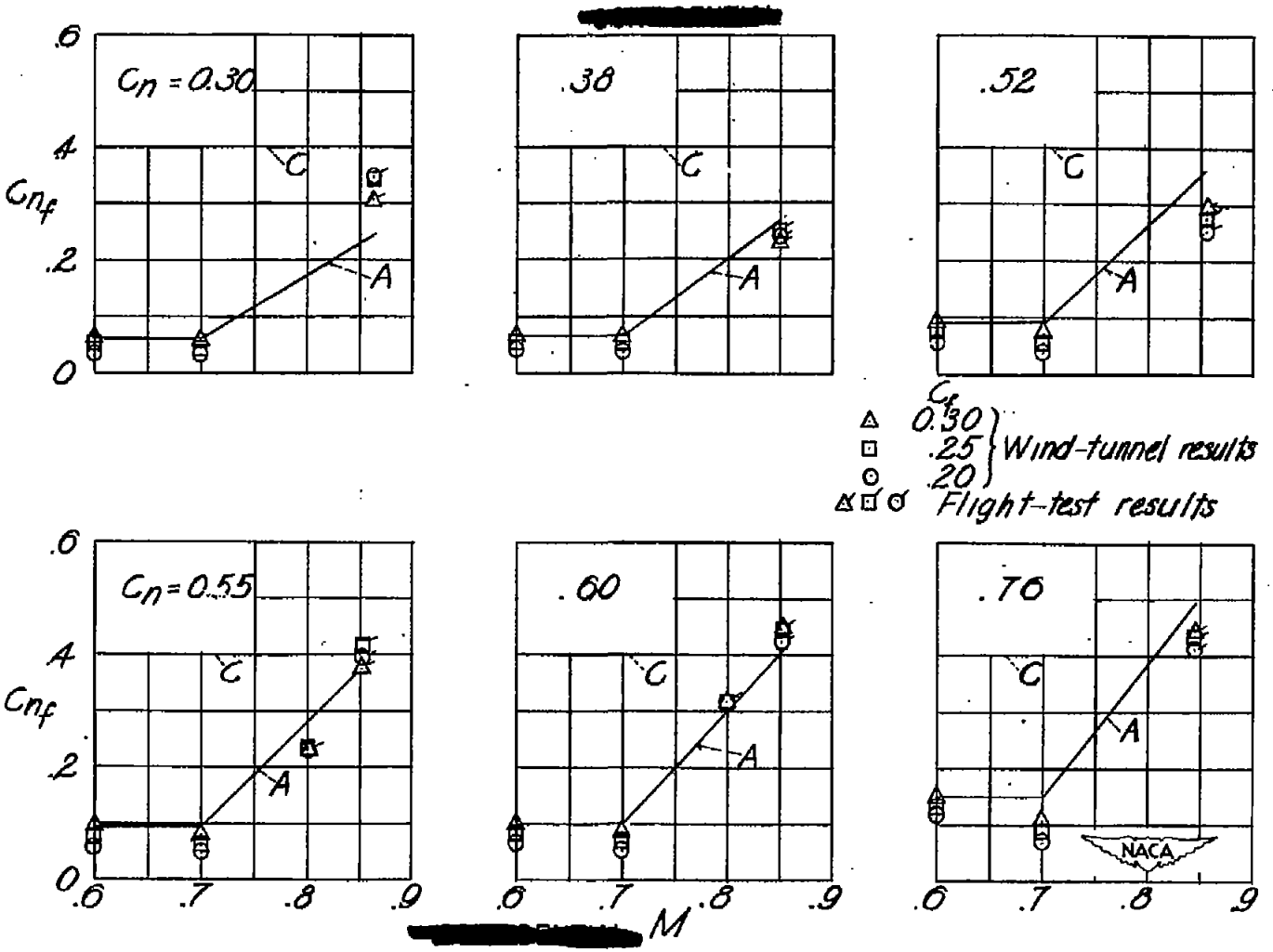

(i) Flight and wind-tunnel results for test airplane having an NACA 65-213 airfoil section.

Figure 3.- Continued.

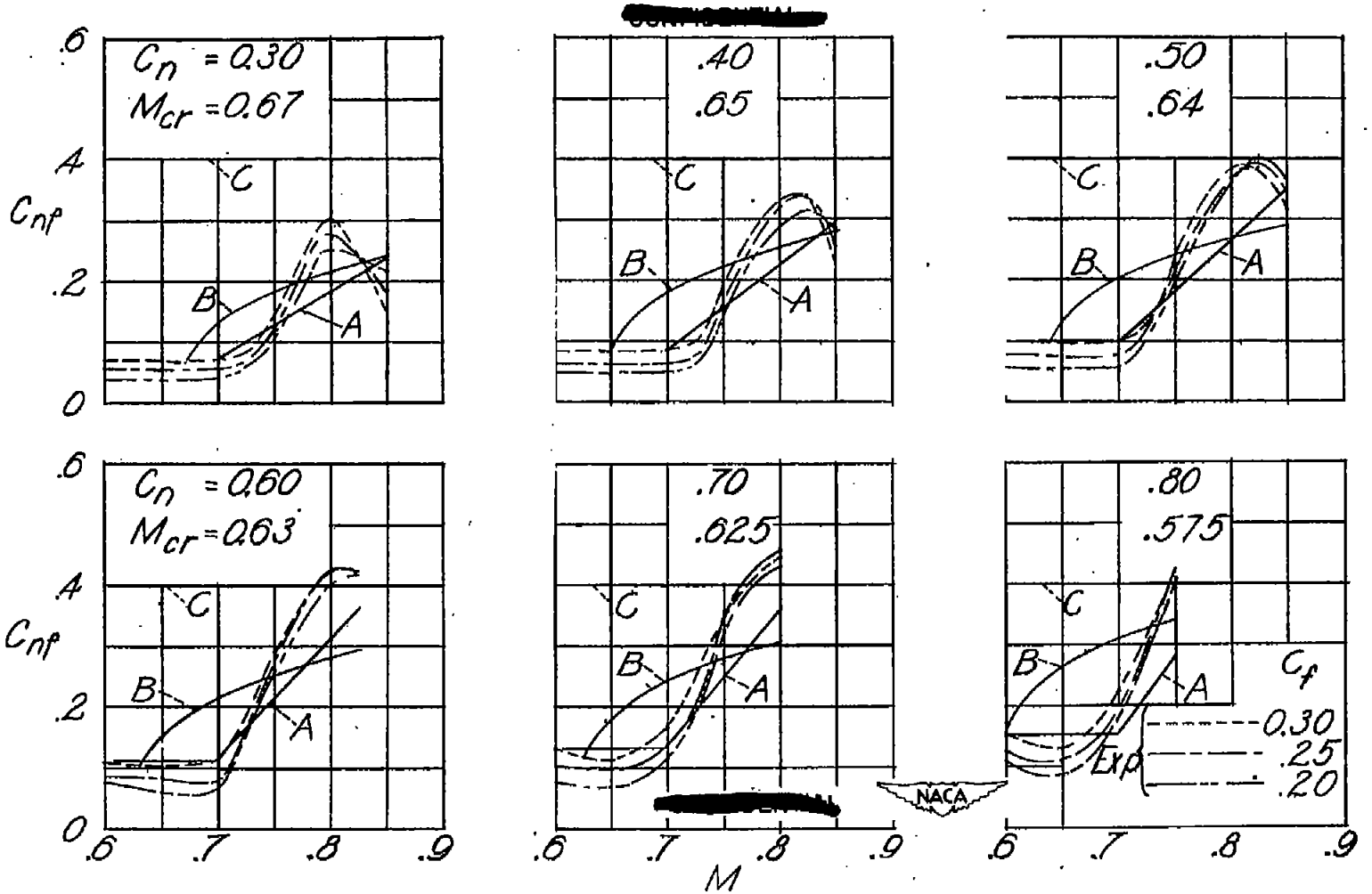

(j) NACA 65-215 (a=0.5) airfoil section.

Figure 3.- Continued.

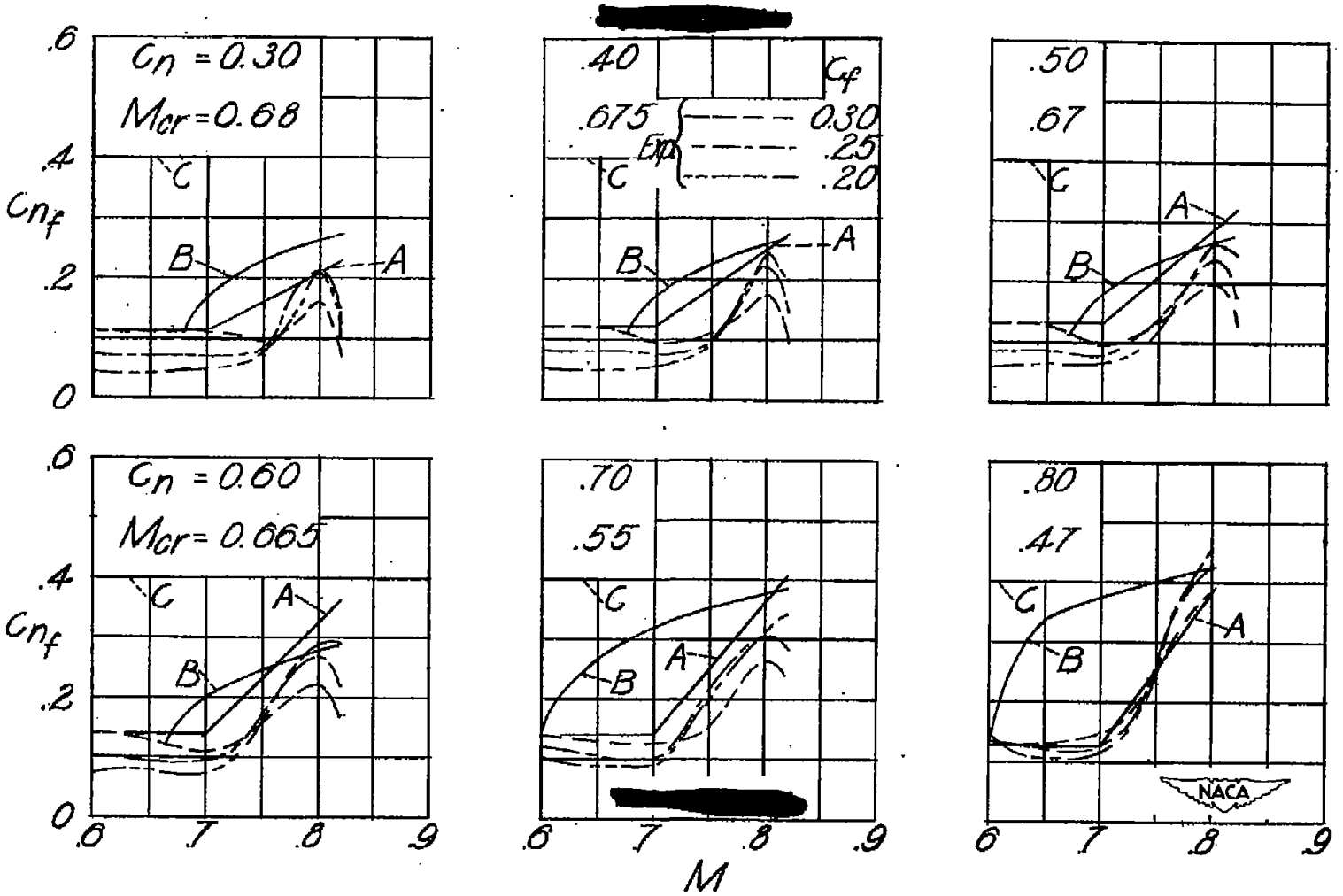

(k) NACA 66,2-215 (a=0.6) airfoil section.

Figure 3.- Continued.

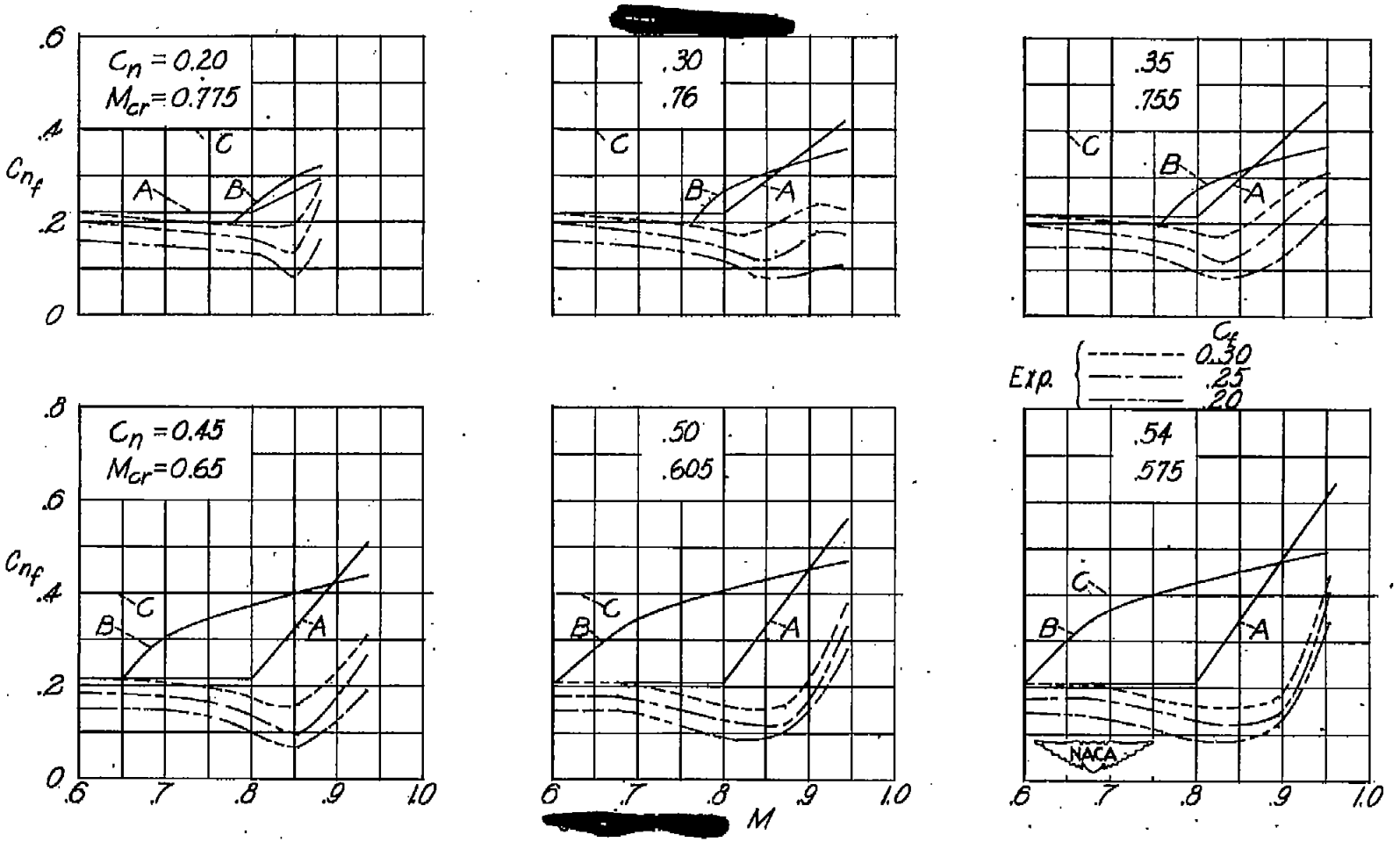

(l) Propeller having an NACA 16-307 airfoil section at 80-percent radius station.

Figure 3.- Continued.

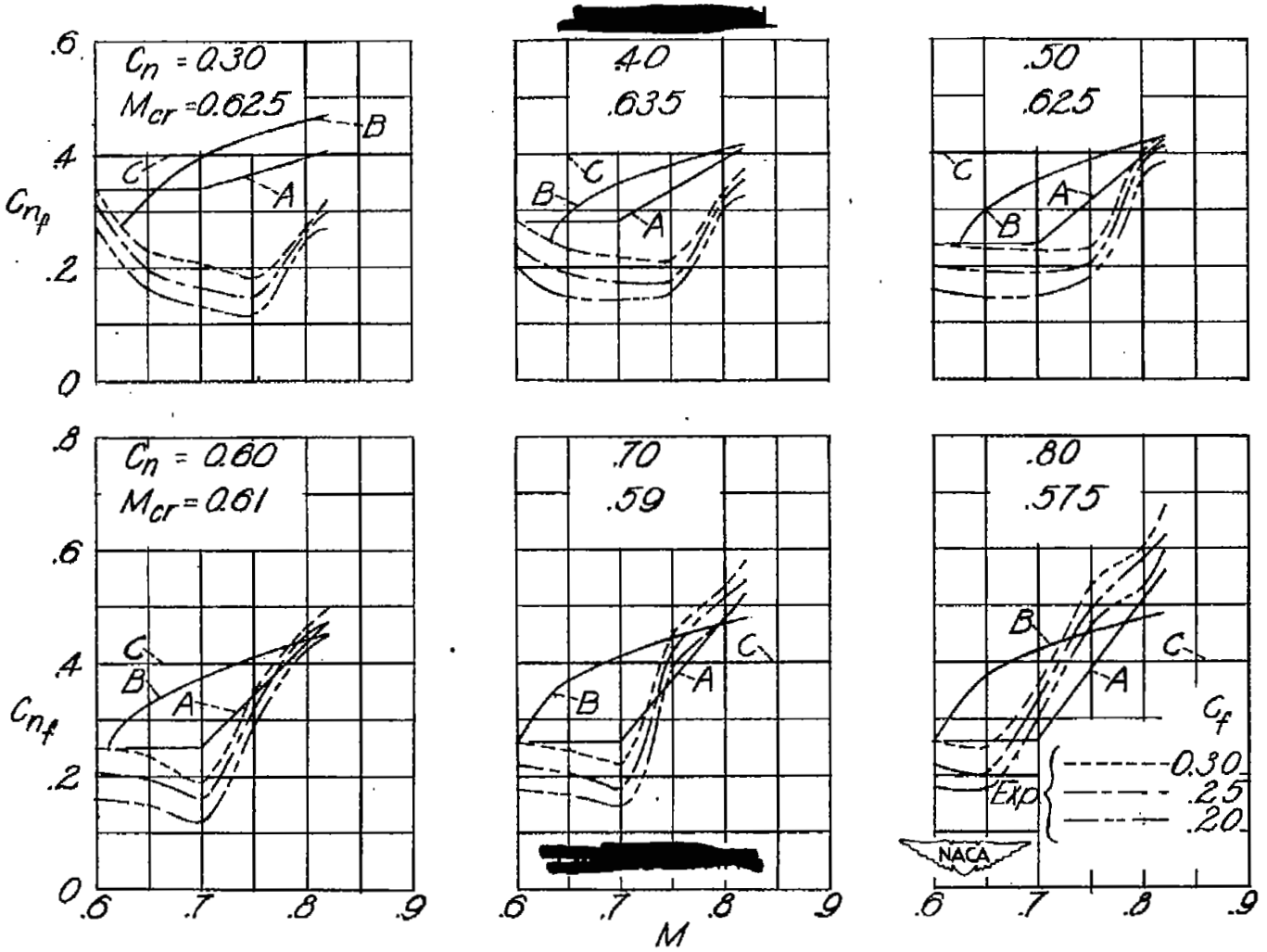

(m) NACA 4415 airfoil section.

Figure 3.- Continued.

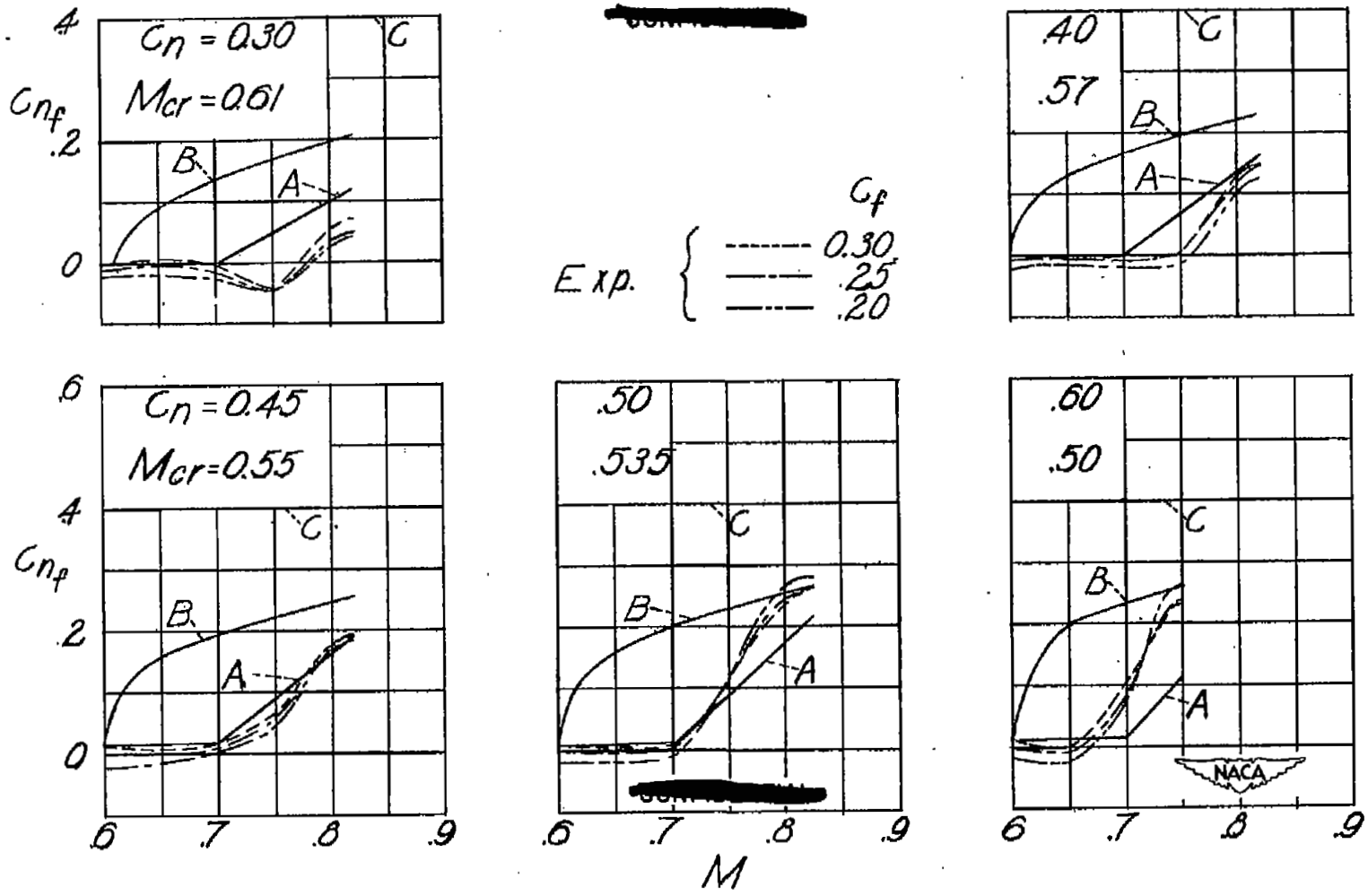

(n) NACA 0015 airfoil section.

Figure 3.- Continued.

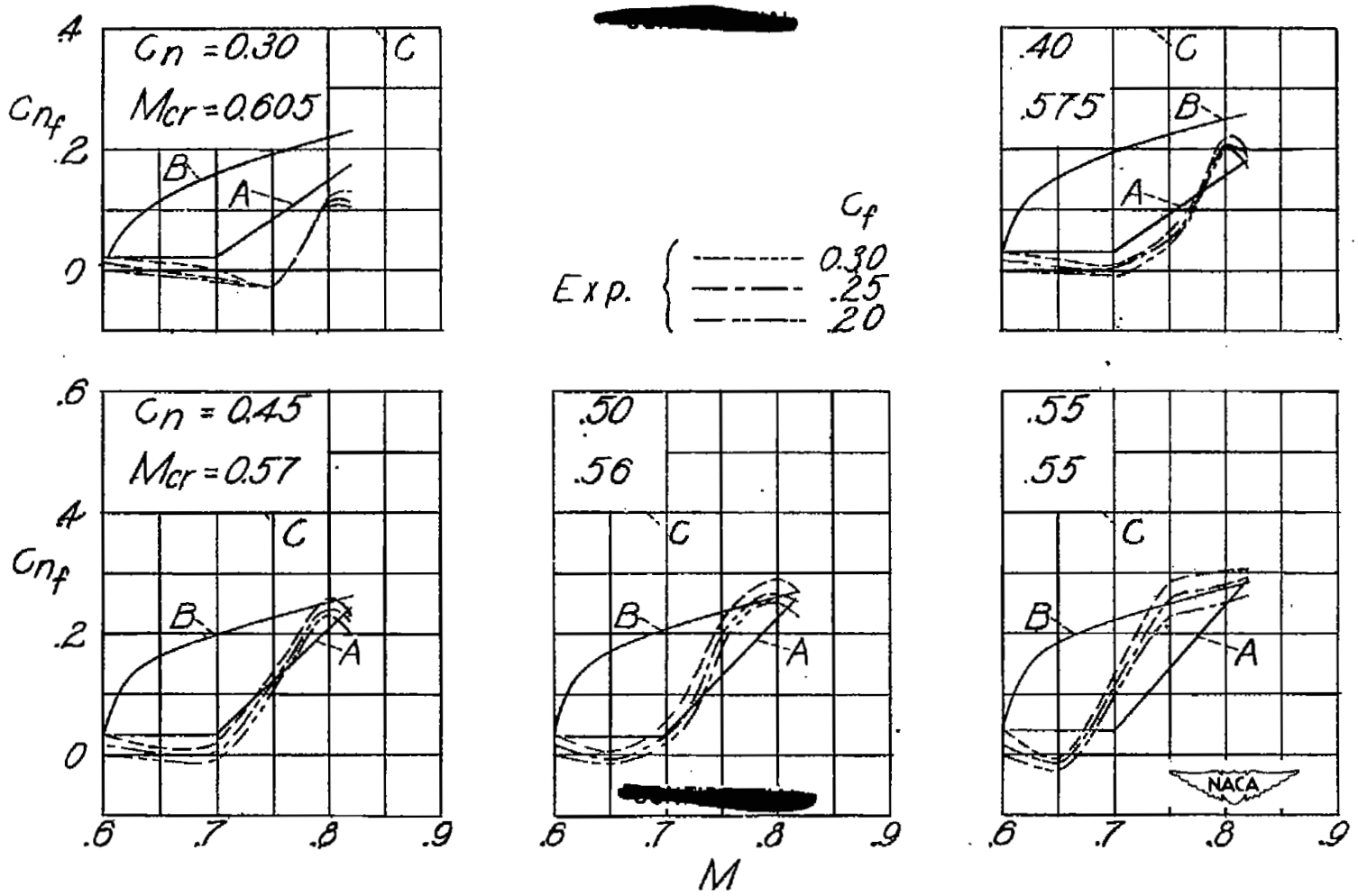

(o) NACA 23015 airfoil section.

Figure 3.- Concluded.

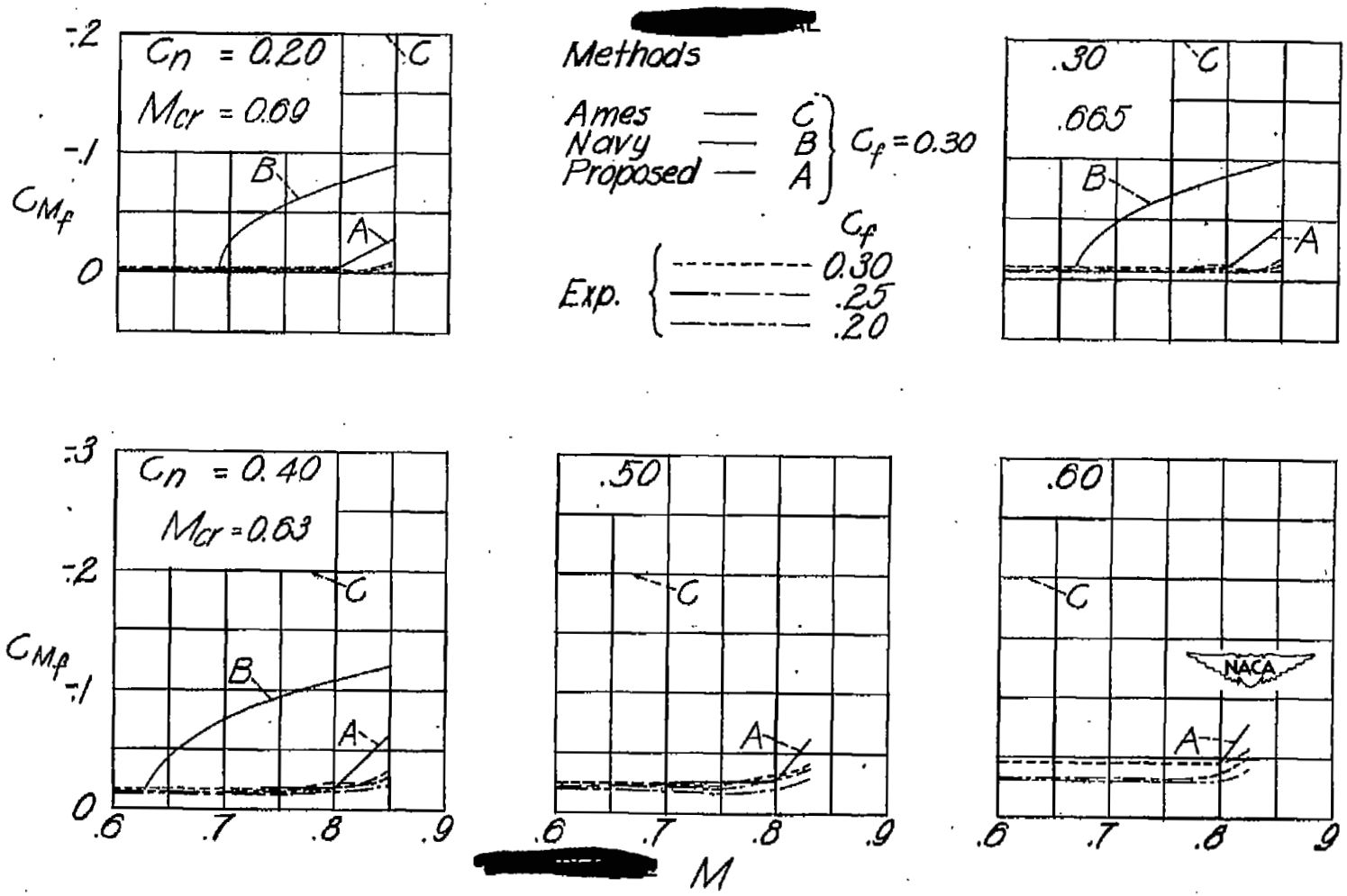

(a) NACA 1S(30)(03)-(30)(03) airfoil section. (Uncorrected results)

Figure 4.- Comparison of experimental and calculated trailing-edge bending-moment coefficients.

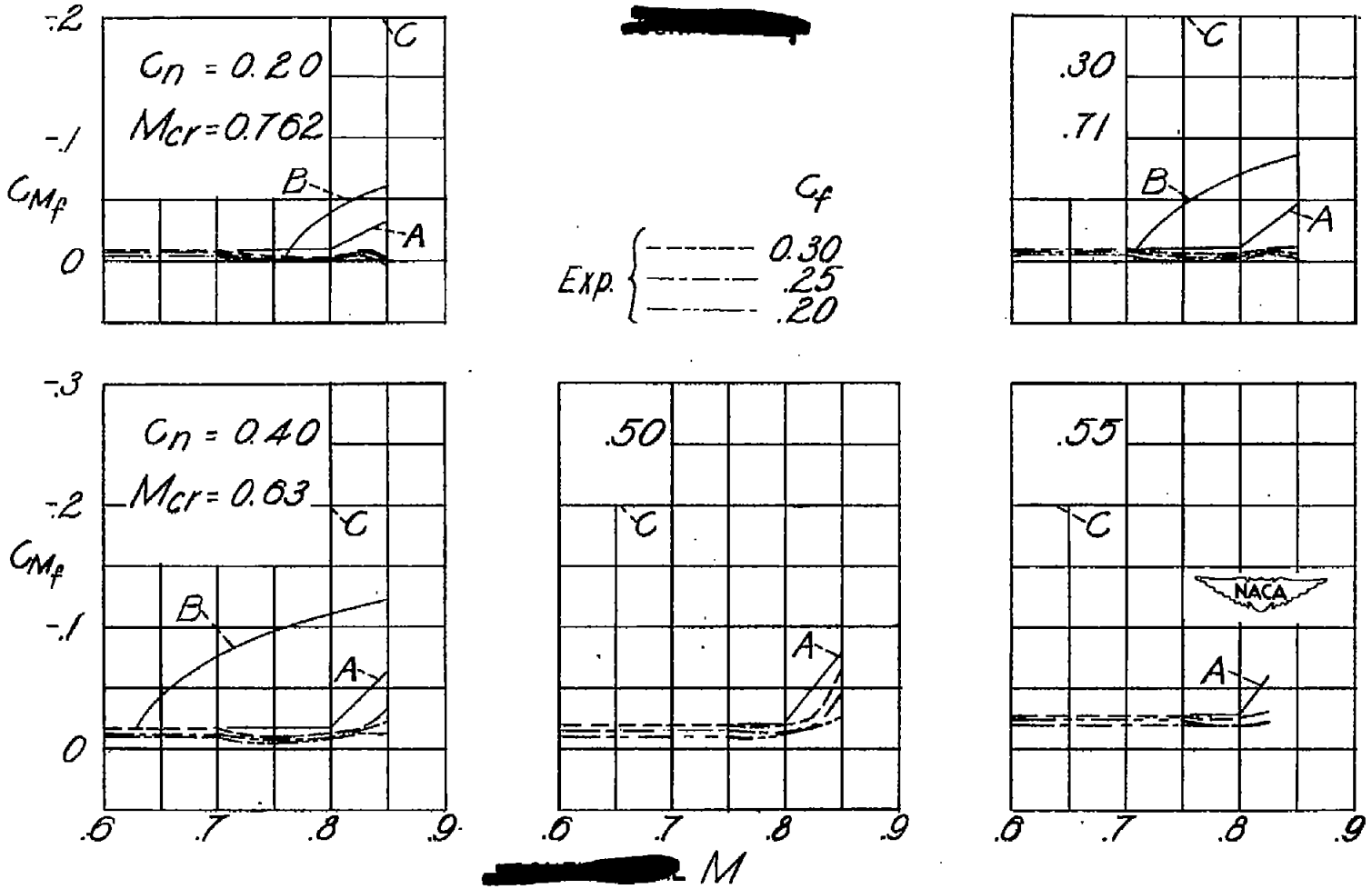

(b) NACA 2S(30)(03)-(30)(03) airfoil section. (Uncorrected results)

Figure 4.- Continued.

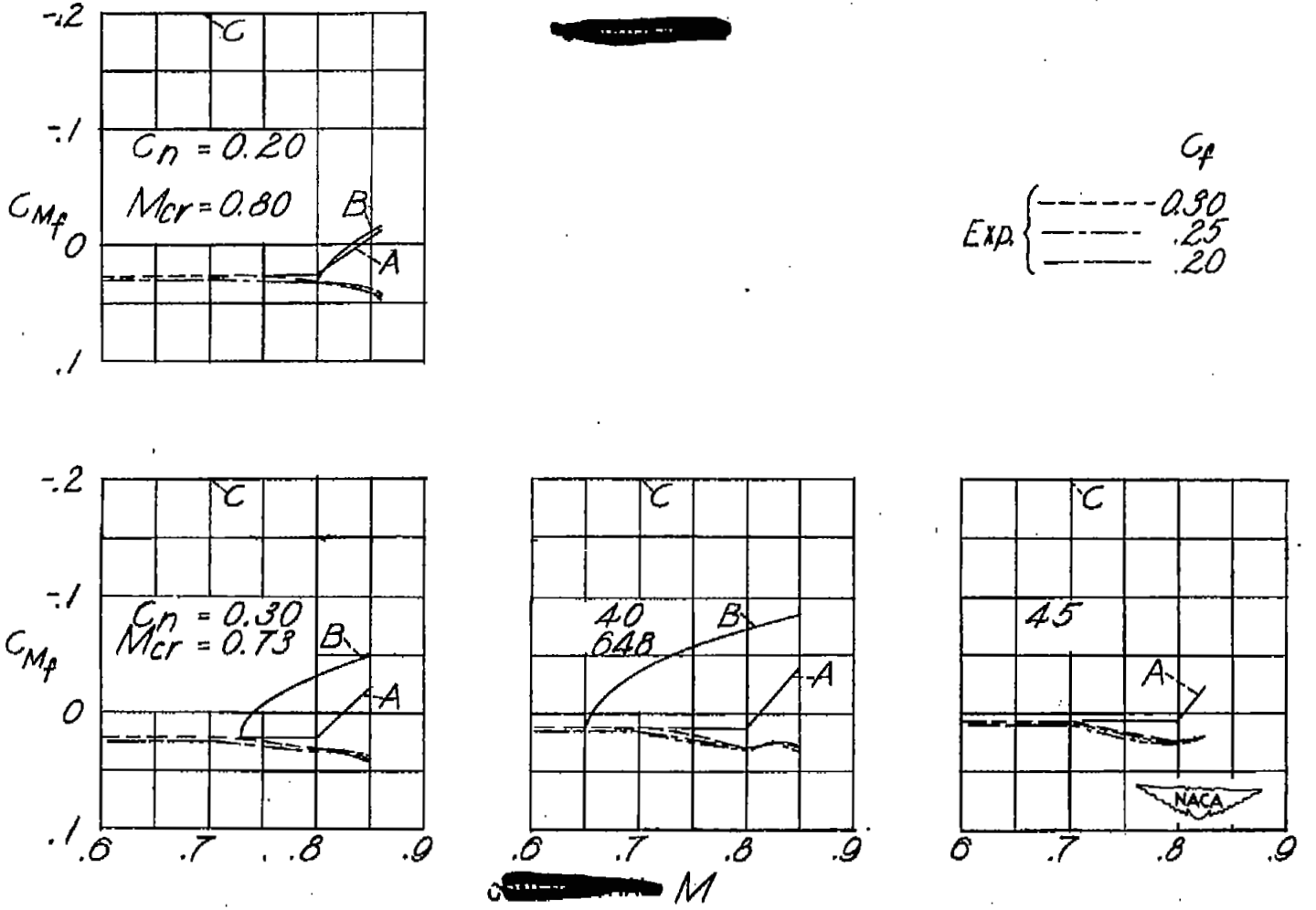

(c) NACA 28(50)(03)-(50)(03) airfoil section. (Uncorrected results)

Figure 4.- Continued.

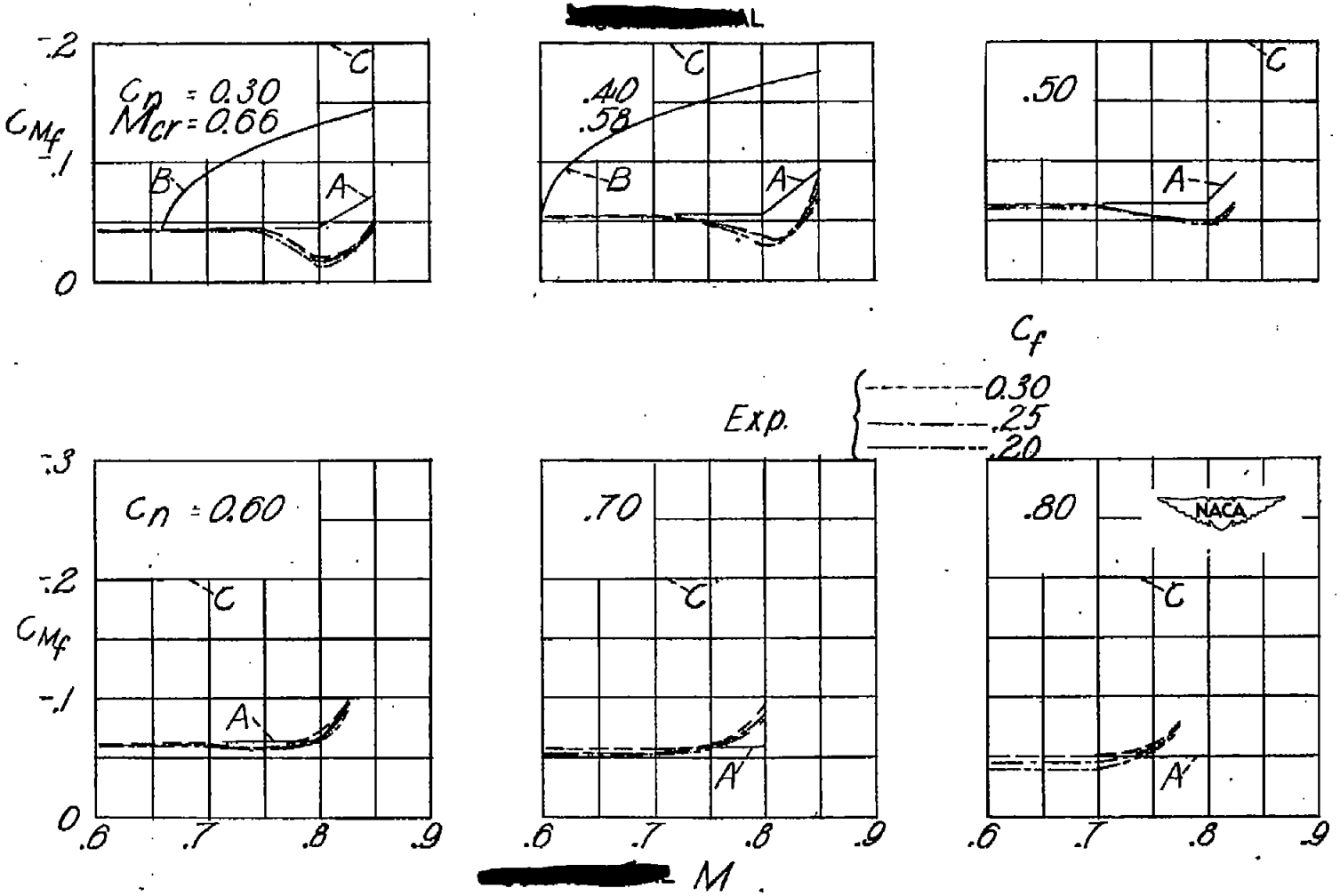

(d) NACA 66-006 airfoil section. (Uncorrected results)

Figure 4.- Continued.

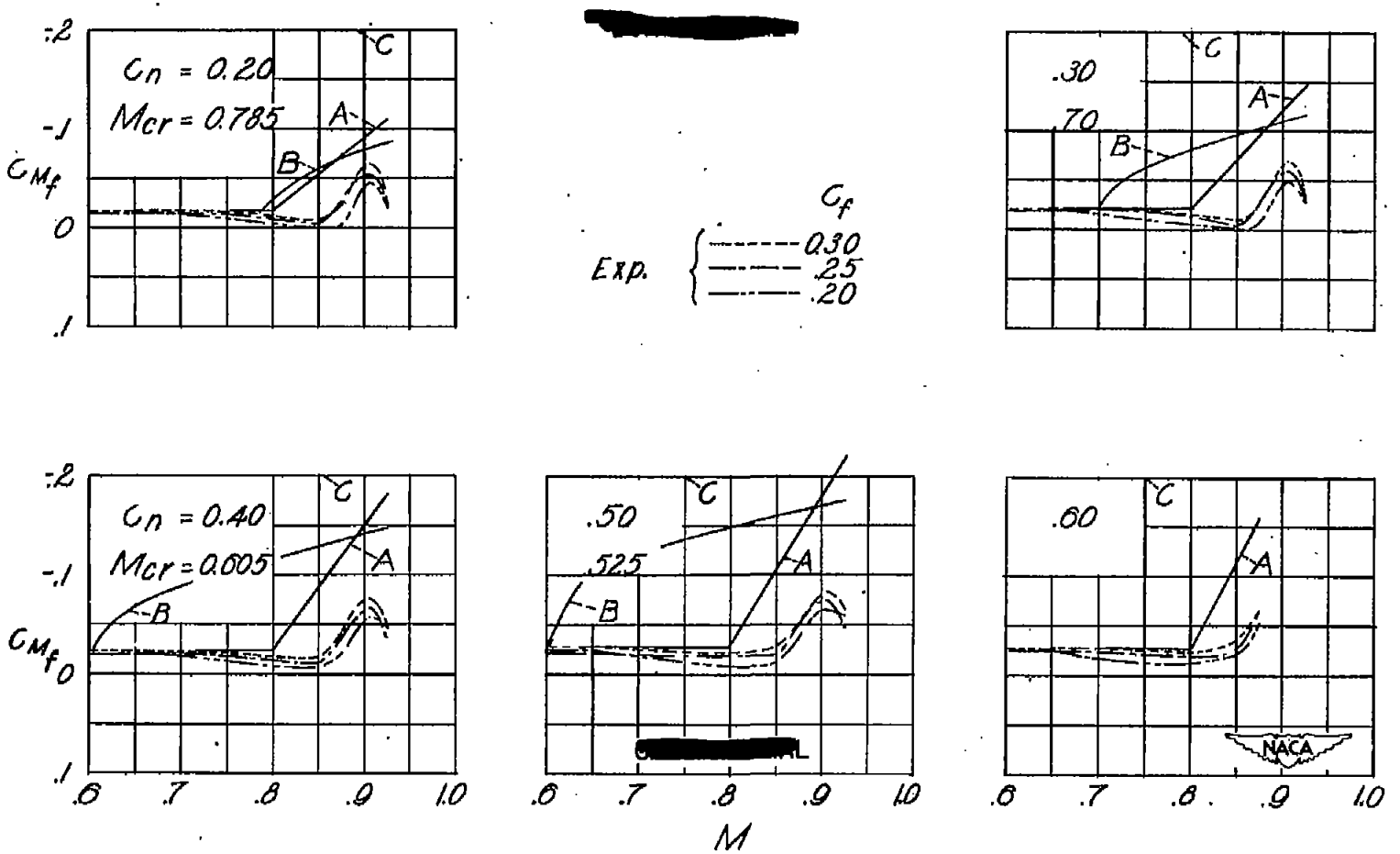

(e) Horizontal-tail model having an NACA 65-108 airfoil section equipped with a 0.30c plain elevator; 40-percent semispan station.

Figure 4.- Continued.

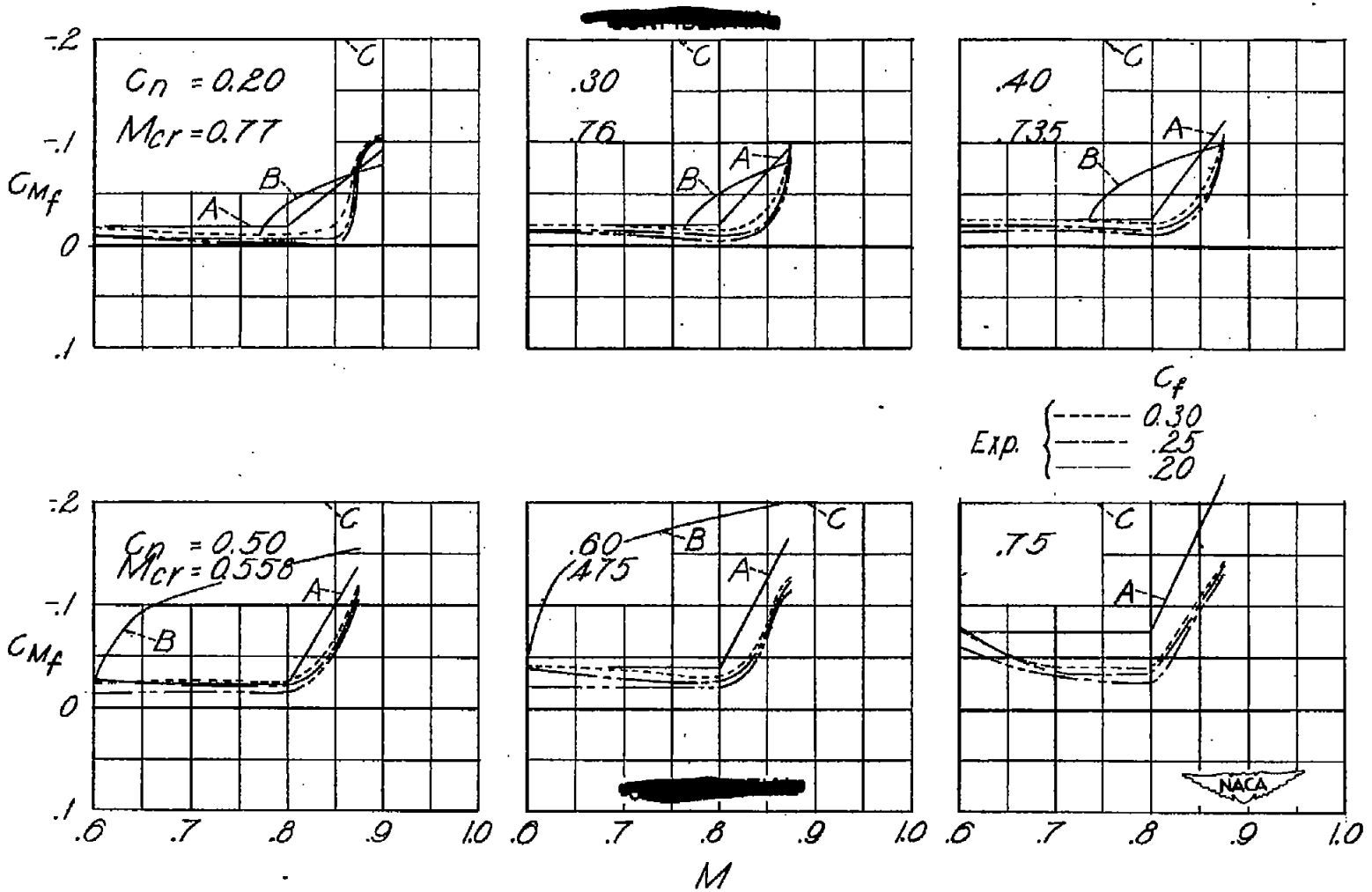

(f) Wing model having an NACA 65-208 airfoil section; 16-percent semispan station.

Figure 4.- Continued.

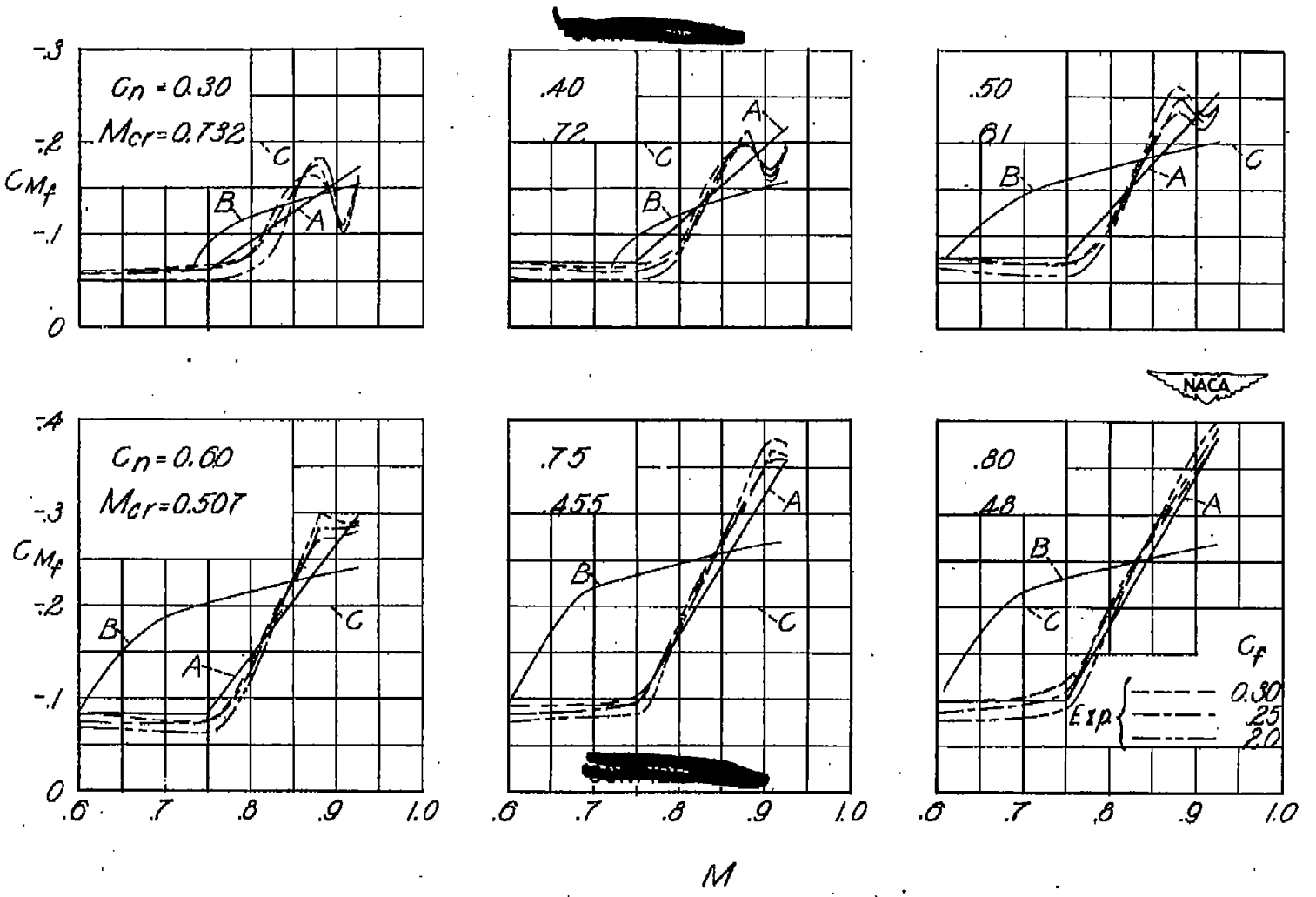

(g) Wing model having an NACA 65-210 airfoil; 30-percent semispan station.

Figure 4.- Continued.

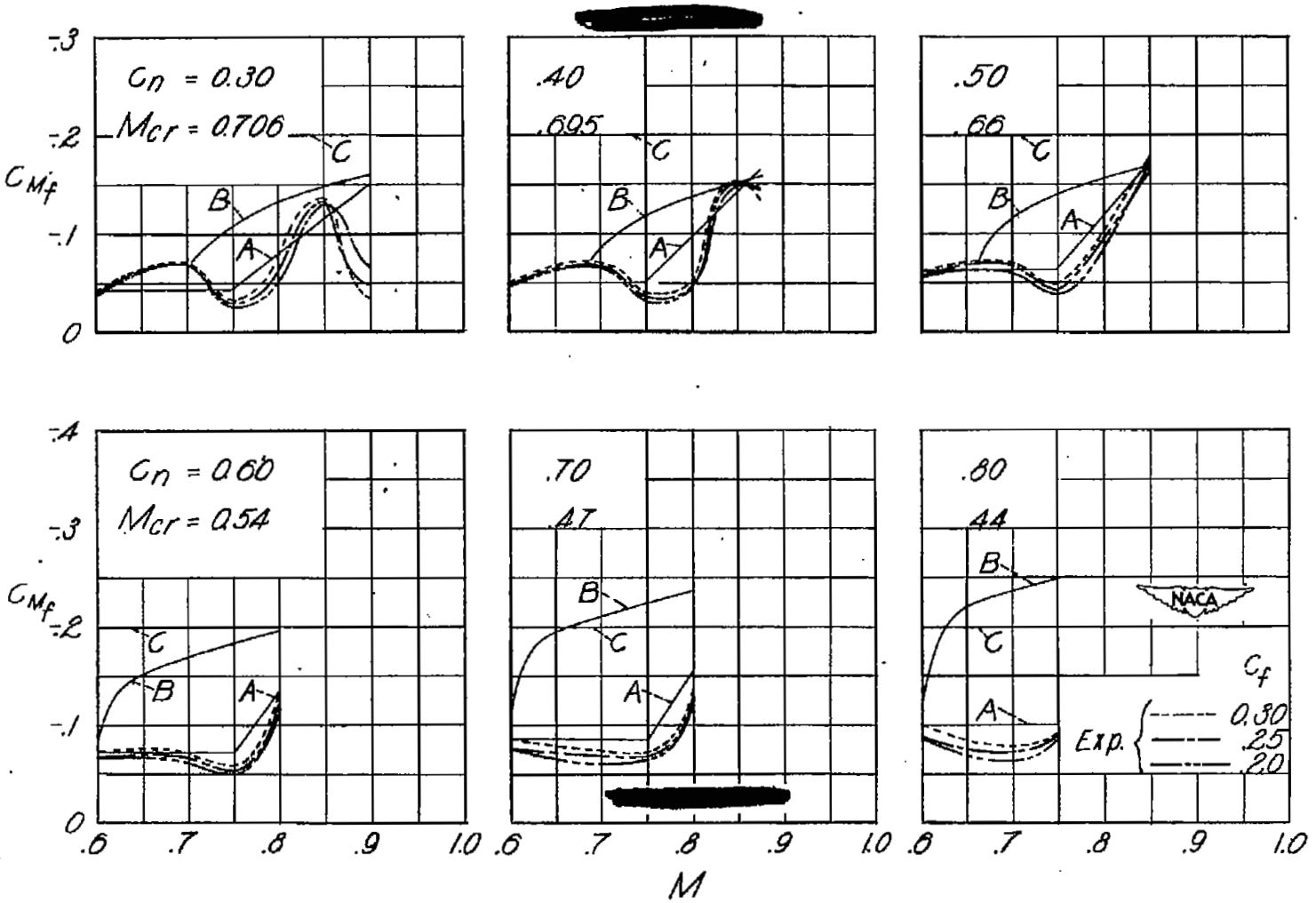

(h) Wing model having an NACA 65-212 airfoil section; 16-percent semispan station.

Figure 4.- Continued.

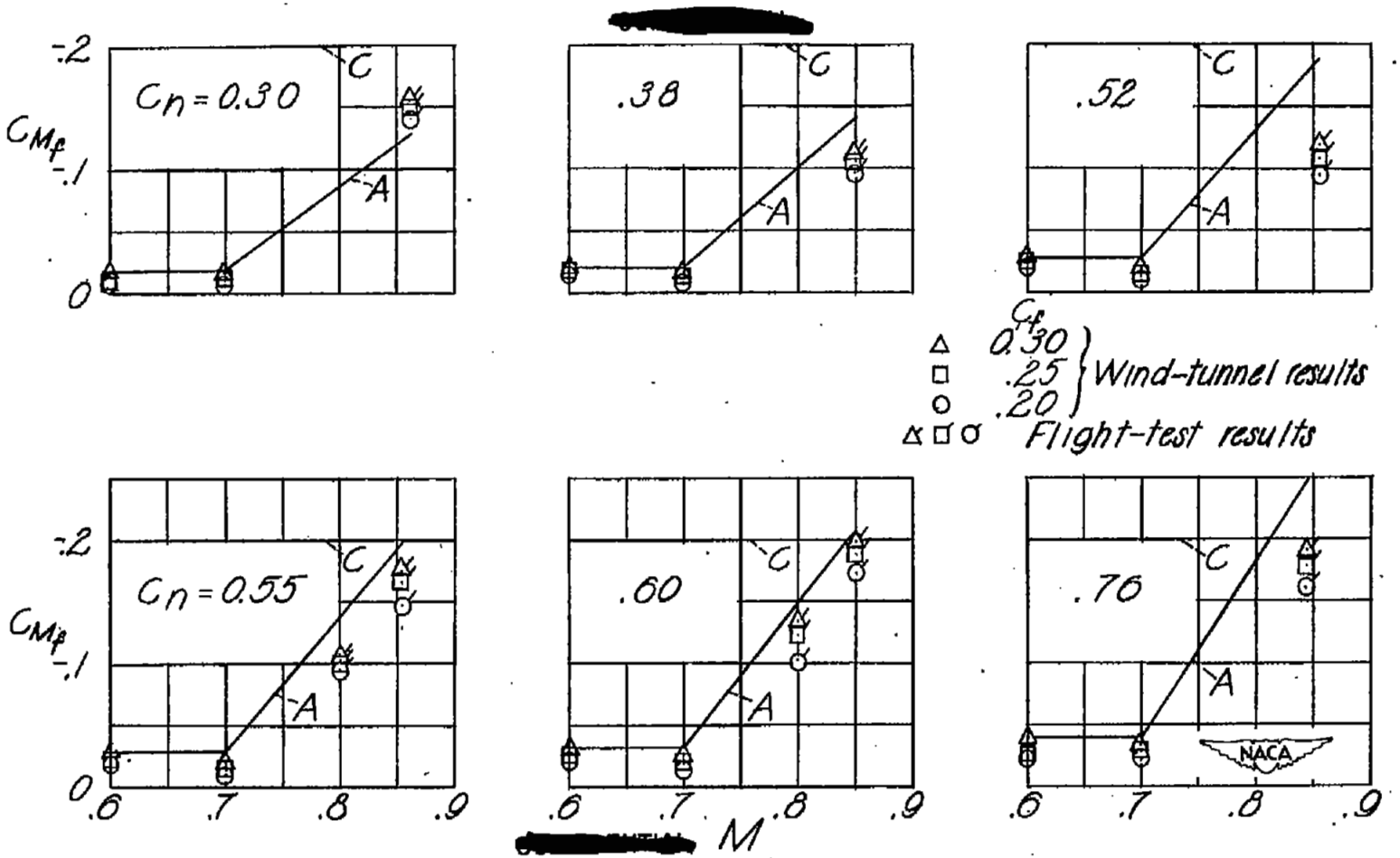

(i) Flight and wind-tunnel results for test airplane having an NACA 65-213 airfoil section.

Figure 4.- Continued.

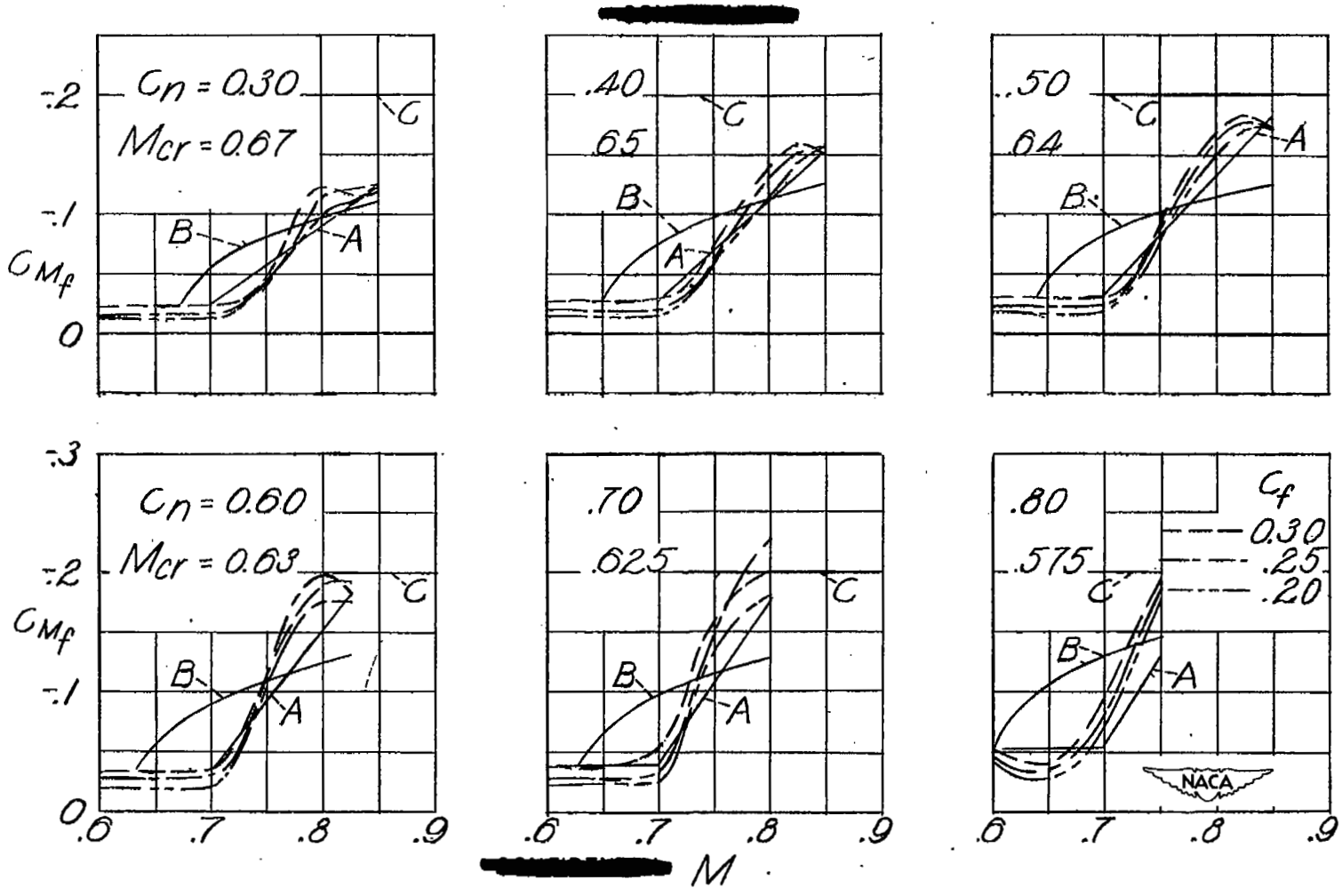

(j) NACA 65-215 (a=0.5) airfoil section.

Figure 4.- Continued.

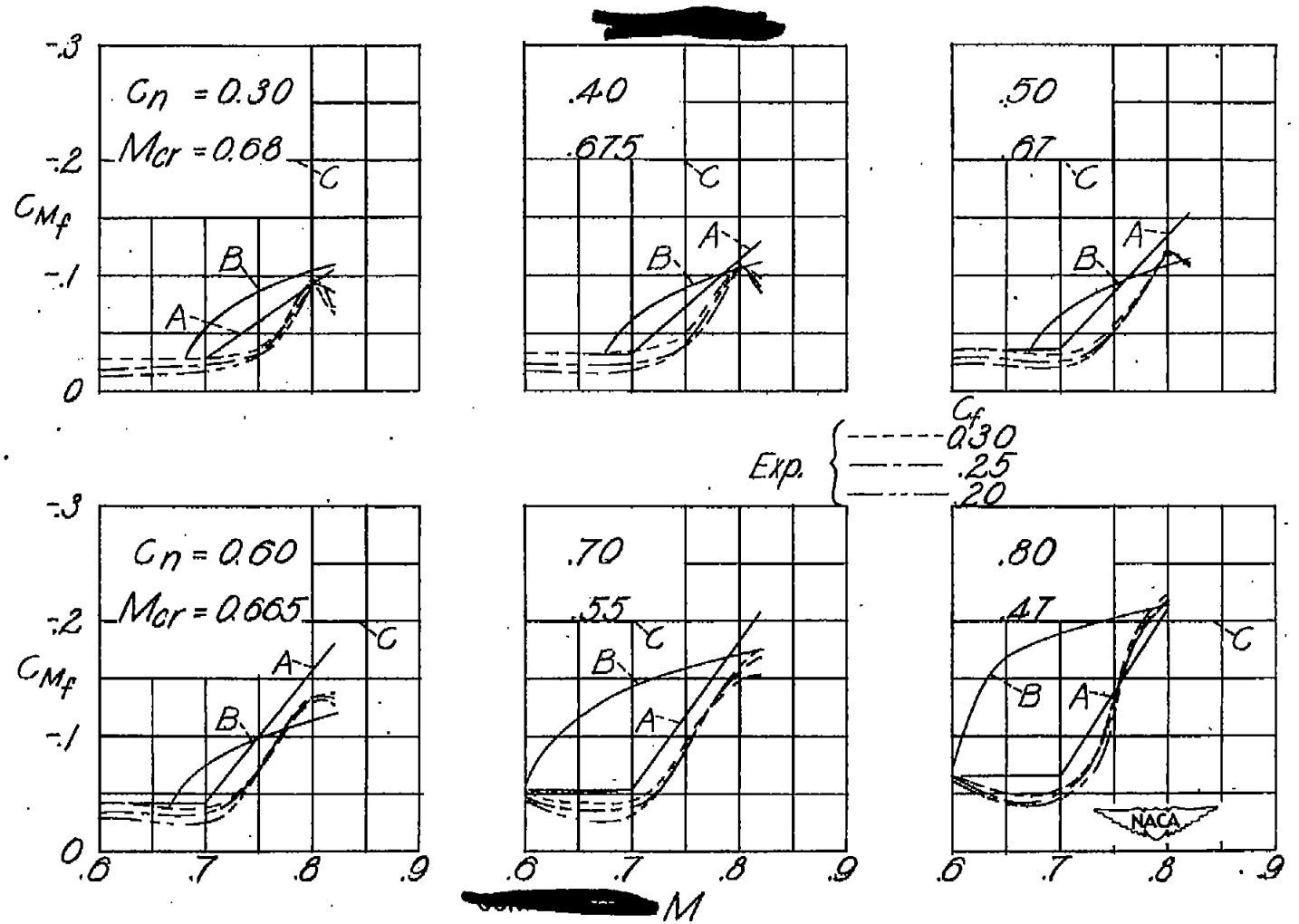

(k) NACA 66,2-215 (a=0.6) airfoil section.

Figure 4.- Continued.

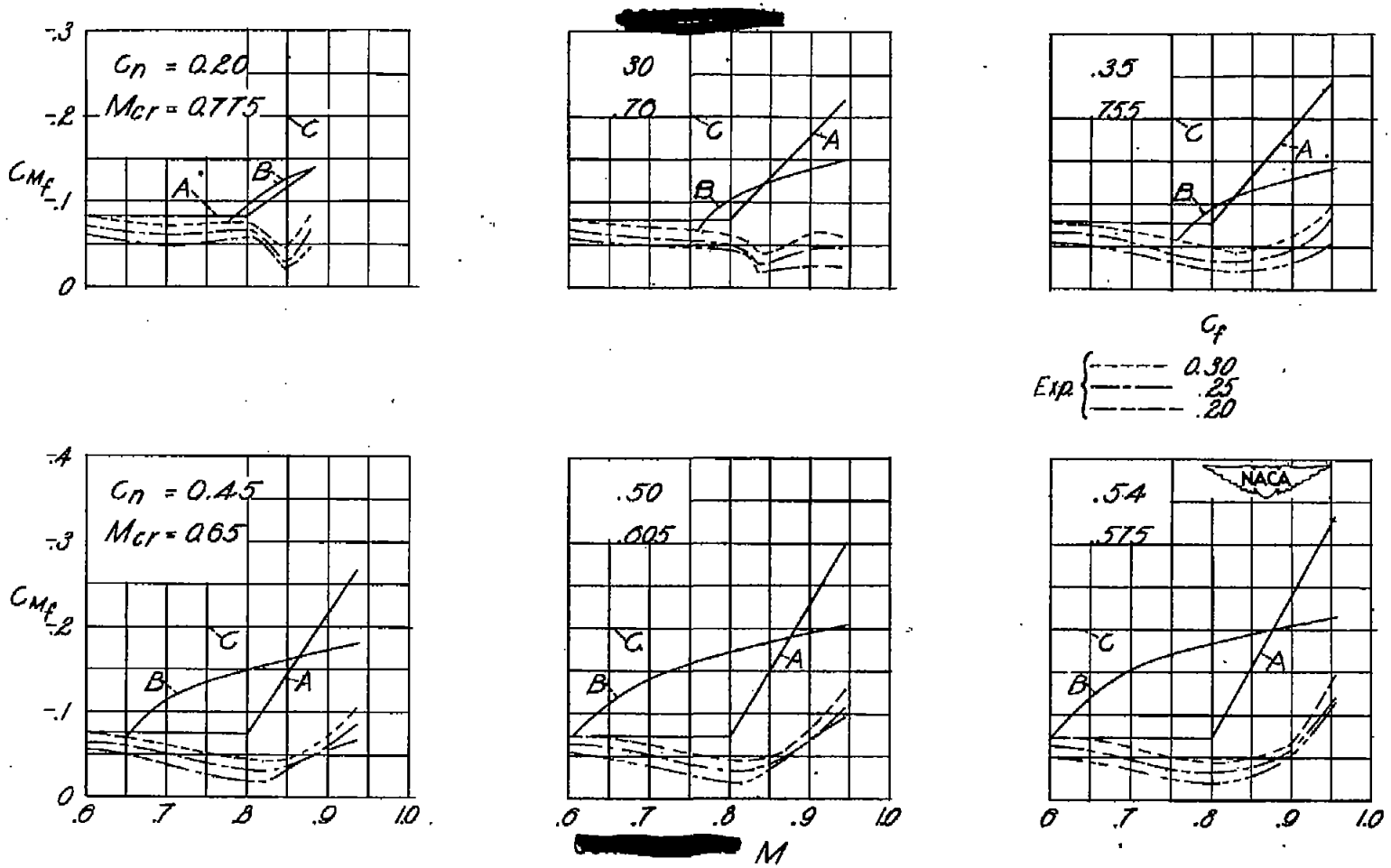

(l) Propeller having an NACA 16-307 airfoil section at 80-percent radius station.

Figure 4.- Continued.

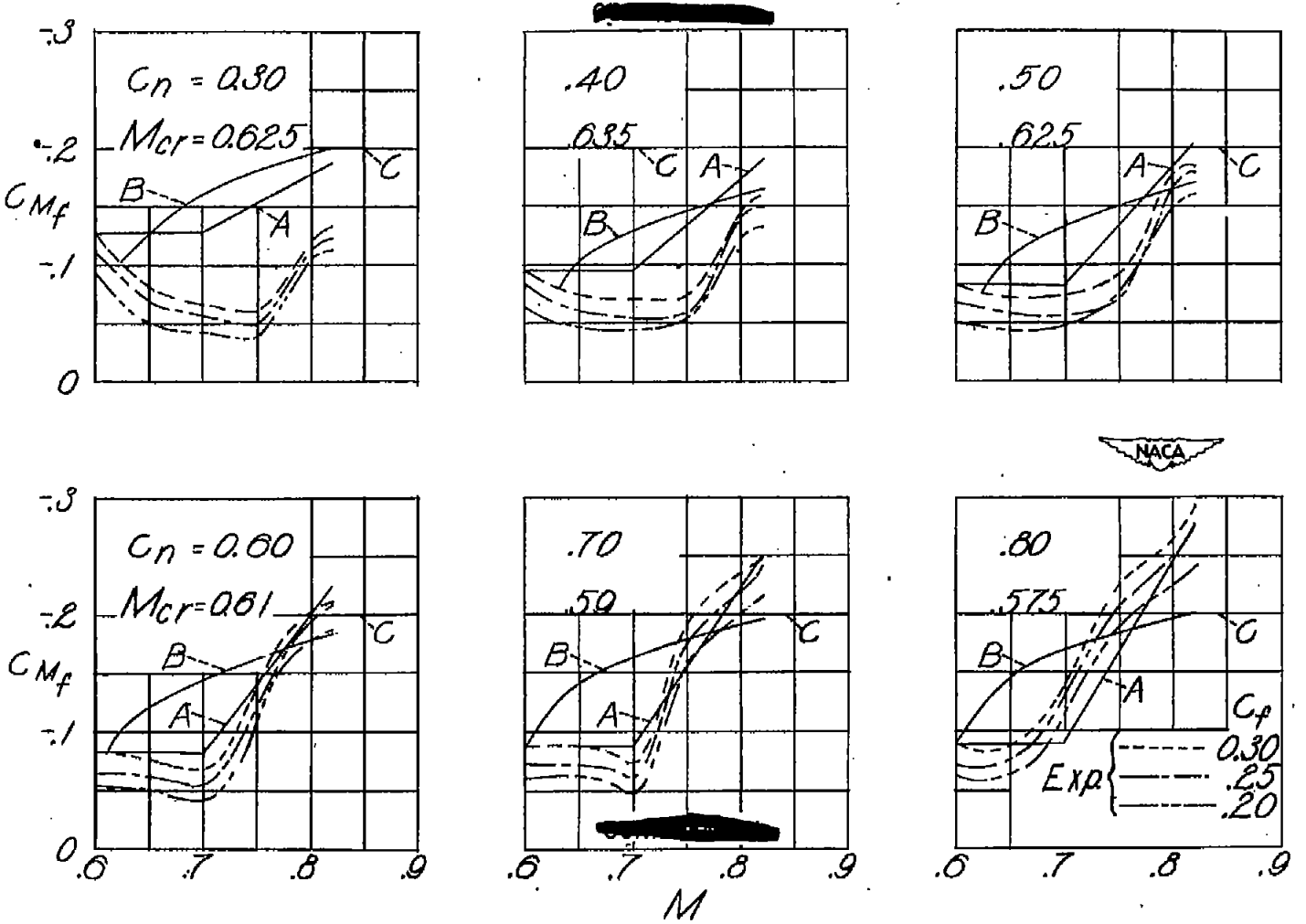

(m) NACA 4415 airfoil section.

Figure 4.- Continued.

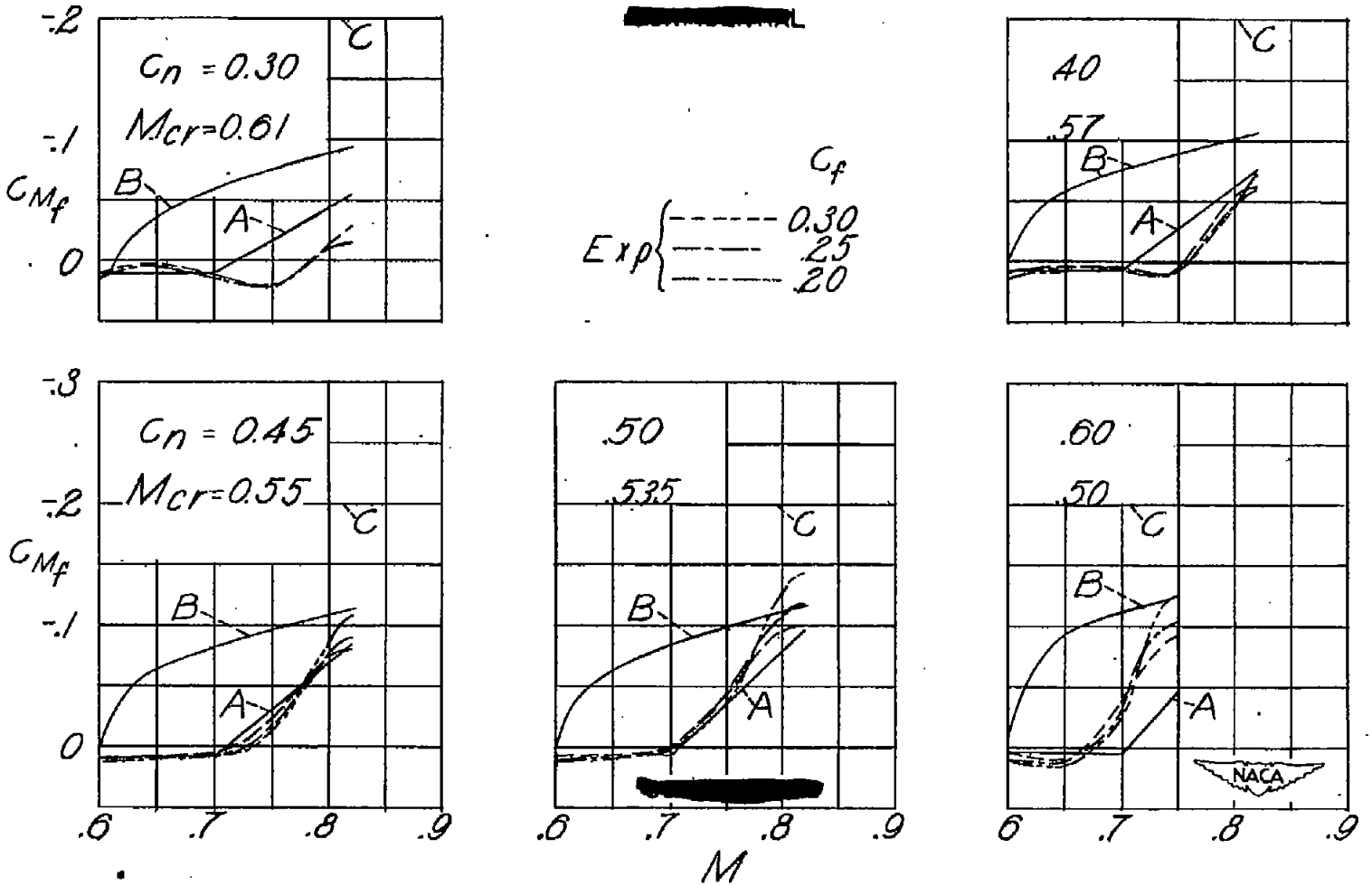

(n) NACA 0015 airfoil section.

Figure 4.- Continued.

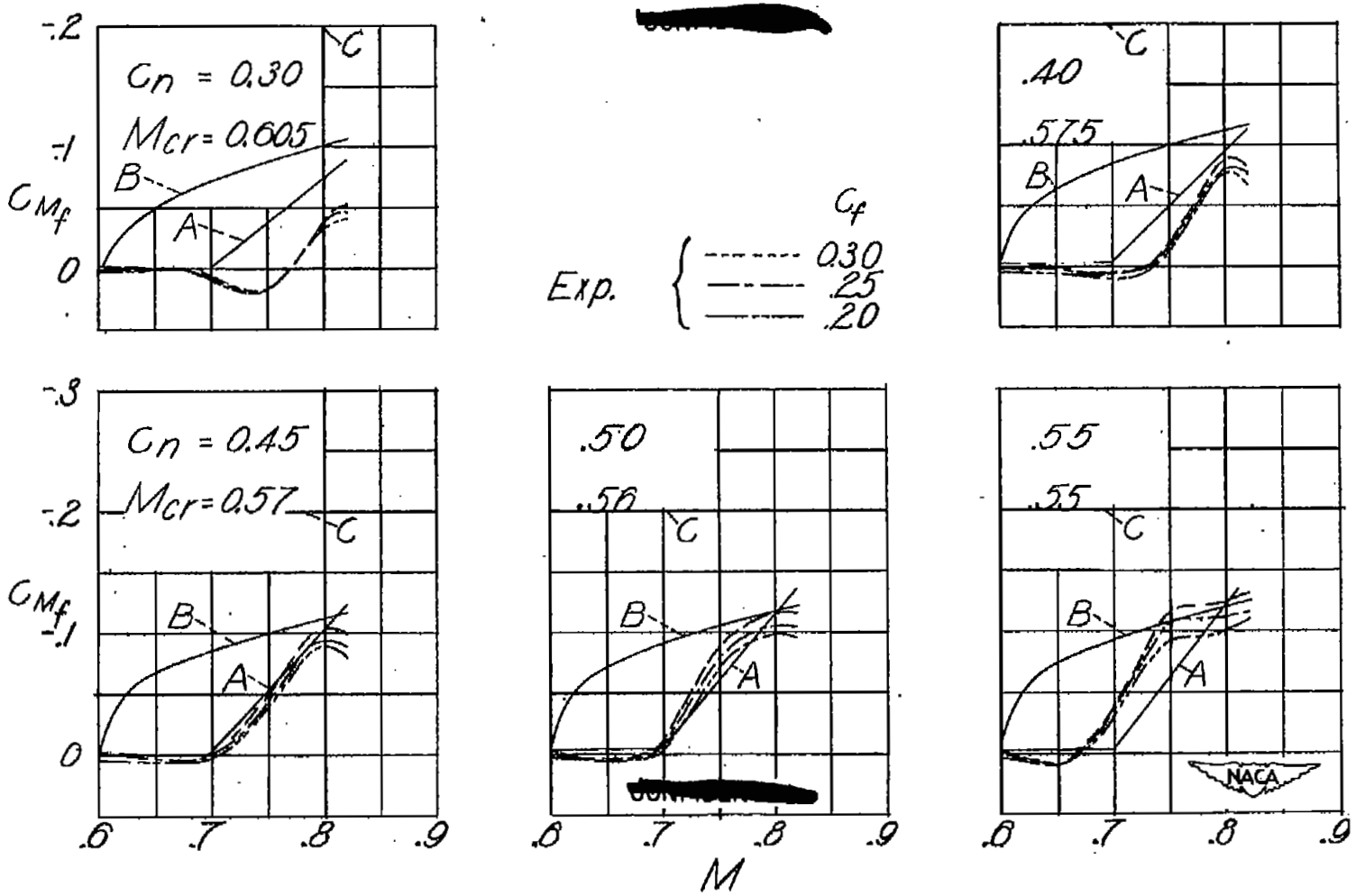

(o) NACA 23015 airfoil section.

Figure 4.- Concluded.